

Supporting Information

Orthogonal assisted tandem reactions for the upgrading of bio-based aromatic alcohols using chitin derived mono and bimetallic catalysts

Francesco Zorzetto,^a Daniel Ballesteros-Plata,^b Alvisè Perosa,^a Enrique Rodríguez-Castellón,^b Maurizio Selva,^{a*} Daily Rodríguez-Padrón^{a*}

The upgrading of a benzyl-type alcohols was explored via an orthogonal tandem sequence comprised of a first oxidative step producing the corresponding aldehydes, and a subsequent reductive amination to achieve both secondary and tertiary amines. To the scope, acetonitrile (ACN) was used as a solvent and a source/precursor of reactant amines, and different heterogeneous catalysts based on Rh and Mo, were designed as mono- and bimetallic systems in the form of metal nanoparticles dispersed on a chitin-derived *N*-doped carbons. A parametric analysis carried out separately for the oxidation and the reductive amination allowed to choose the best performant catalyst for both the reactions of the tandem process. A one-pot two-step protocol was implemented accordingly: as an example, benzyl alcohol was quantitatively and selectively oxidised to benzaldehyde (>99%) which in turn, was converted to *N*-benzylethanamine (66%) or *N*-benzyl-*N*-ethylethanamine (60%) in the presence of [Rh(5%)-N/C - Mo(5%)]-N/C or [Rh(3%)-N/C - Mo(5%)]-N/C as catalysts, respectively. The tandem sequence proved successful also for other bio-based benzyl-type alcohols that afforded the corresponding secondary/tertiary amines in yields up to 53-93%. Overall, the study proved the viability of an innovative method aimed not only at process intensification for multistep synthesis, but also at the valorization of substrates (alcohols) and biopolymers (chitin) derived from biomass

Materials characterization

Mo(5%)-N/C: The Mo-N/C sample, comprising molybdenum nanoparticles supported on *N*-doped carbons, was synthesized using 1 mmol of (NH₄)MoO₄ precursor to achieve a final Mo loading of 5 wt.%. Fig. 16 below presents the characterization results for this sample, including N₂-physisorption, XRD and XPS analyses.

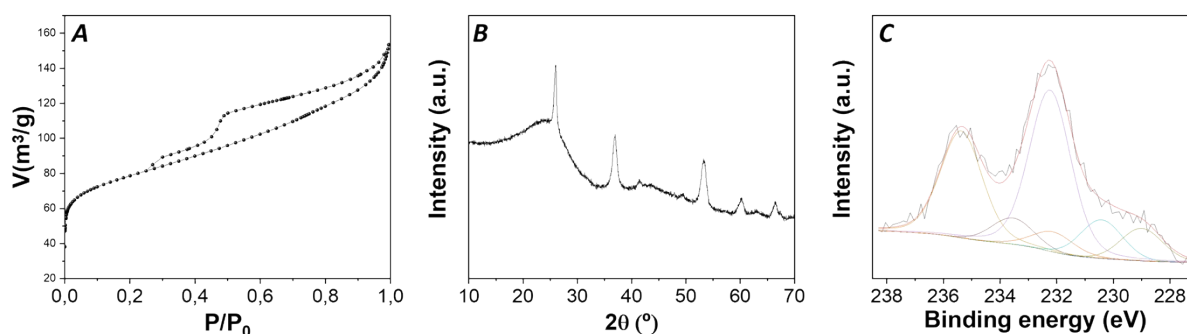


Figure S1: Characterization of Mo(5%)-N-C sample through A: N₂-physisorption, B: XRD and C: Mo 3d core level

spectrum.

XRD: The crystal structure and arrangement of the synthesized sample were analyzed using XRD. In the XRD pattern of the Mo-N/C sample (as well as for the Ni, Co, and Fe samples, as shown in the XRD diffractograms in the appendix), a distinct peak at approximately 25° was observed. This peak was attributed to the (002) crystallographic plane, related to the parallel stacking of graphene-like sheets. Moreover, a weak peak was also detected at 43° which was assigned to the (100) crystallographic plane of graphitic carbon arranged in a honeycomb network. The broad shape of this peak was due the amorphous nature of the synthesized samples which was ascribed to two factors: i) the thermal protocol employed and ii) the N-doping in the carbonaceous structure, which introduced defect sites. As reported in the literature,¹⁸ amorphous materials may offer advantages in terms of catalytic activity compared to crystalline solids because of the greater structural flexibility. The XRD diffractogram of the Mo-based system showed other well-defined signals around 26, 35, 39, 51, 59 and 66°. The higher intensity of the peaks at ca. 26, 35 and 51°, most likely indicated the presence of MoO₂ species along with a minor contribution of MoO₃, as suggested from the bands at 39, 59, and 66°. These findings were indicative of the coexistence of various molybdenum species in the sample.

N₂-physisorption: The textural properties of the samples were examined through N₂-physisorption analysis. The observed isotherm exhibited a Type IV pattern, and the adsorption hysteresis was classified as Type II, indicating the formation of mesoporous materials and the presence of disordered networks. Detailed textural properties of the catalysts, such as surface area, pore diameter, and pore volume, are shown in Table 9.

Table S1: N₂-physisorption parameters for the Mo(5%)-N/C sample.

Material Sample	S _{BET} [m ² /g] ^a	D _{BJH} [nm] ^b	V _{BJH} [cm ³ /g] ^c
Mo(5%)-N/C	285	2.9	0.2

a: S_{BET}: specific surface area was calculated by the Brunauer-Emmett-Teller (BET) equation.

b: D_{BJH}: mean pore size diameter was calculated by the Barret-Joyner-Halenda (BJH) equation.

c: V_{BJH}: pore volumes were calculated by the Barret-Joyner-Halenda (BJH) equation.

XPS: The chemical properties and composition of the synthesized materials were assessed through XPS analysis. The results, illustrated in Fig. 17, confirmed the presence of metal entities incorporated onto the surface of the N-doped carbonaceous supports.

Mo 3d XPS region of the Mo-N/C sample, was deconvoluted into multiple contributions, at 229.0, 230.4, 232.3, 232.4, 233.5, and 235.3 eV. According to the literature assignments,¹⁸ the signals at binding energies of 229.0 and 232.4 eV were attributed to Mo^{δ+} (0 < δ < 4) entities in molybdenum nitride, suggesting the formation of Mo-N bonds. Additionally, the peaks at 230.4 and 233.5 eV were associated to the doublet Mo 3d_{5/2} and Mo 3d_{3/2} of Mo(IV) entities in MoO₂, while the contributions at 232.3 and 235.3 eV were assigned to the doublet Mo 3d_{5/2} and Mo 3d_{3/2} of Mo(VI) entities in MoO₃. XPS data indicated a higher content of MoO₃ on the material surface in comparison with MoO₂, whereas XRD suggested a higher content of MoO₂ in the bulk sample. This implies a different composition between the surface and the bulk of the catalytic material. Overall, both XRD and XPS characterization analyses of Mo(5%)-N/C were consistent with the formation of core-shell architectures, wherein a core primarily composed of MoO₂ was enveloped by MoO₃, with a minor presence of Mo-N groups.

XPS analysis of the C 1s, N 1s, and O 1s regions of the Mo(5%)-N/C sample is shown in Figure 17.

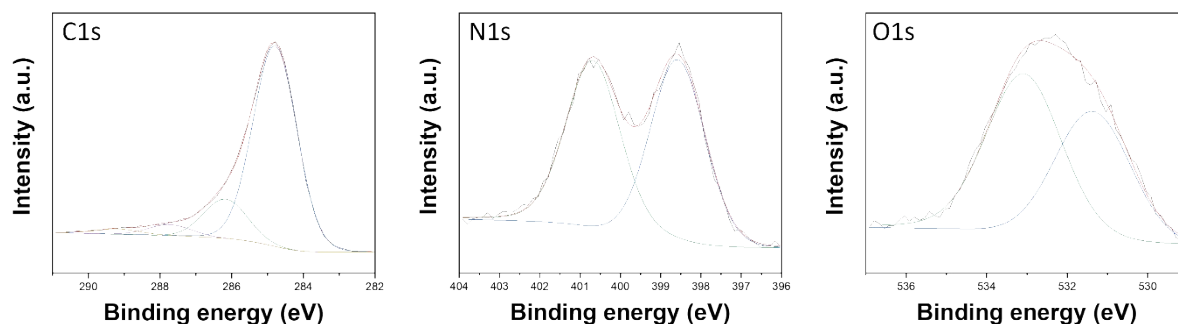


Figure S2: XPS spectra of C 1s (A), N 1s (B), and O 1s (C) regions of the Mo(5%)-N/C sample.

The high-resolution C 1s spectrum of the Mo-N/C sample was deconvoluted into four distinct contributions at approximately 284.7, 286.3, 287.8, and 289.3 eV, corresponding to C-C/C=C bonds (graphitic and aromatic carbon), C-OH, C-N/C-O-C and C=O bonds, respectively. Furthermore, the N 1s core level spectrum exhibited the presence of two primary contributions at around 398.6 and 400.8 eV, attributed to pyridinic and pyrrolic groups, respectively. Lastly, the O 1s XPS region of the prepared materials revealed two contributions at 531.4 and 533.1 eV, associated with lattice oxygen in metal oxides and adsorbed/bonded water, respectively.¹⁸

HRTEM images are displayed in Fig. 18. The presence of well-defined laminar structure of the carbonaceous support was noticed, with multiple layers of N-doped carbon stacked on top of each other. HRTEM images confirmed the presence of uniformly distributed molybdenum nanoparticles with an average diameter of (31±2) nm. Additionally, micrographs and mapping analysis provided evidence of the formation of highly dispersed metallic entities throughout the sample. Though, some metal agglomeration was observed (Fig. 18 ('Mo'), top right).

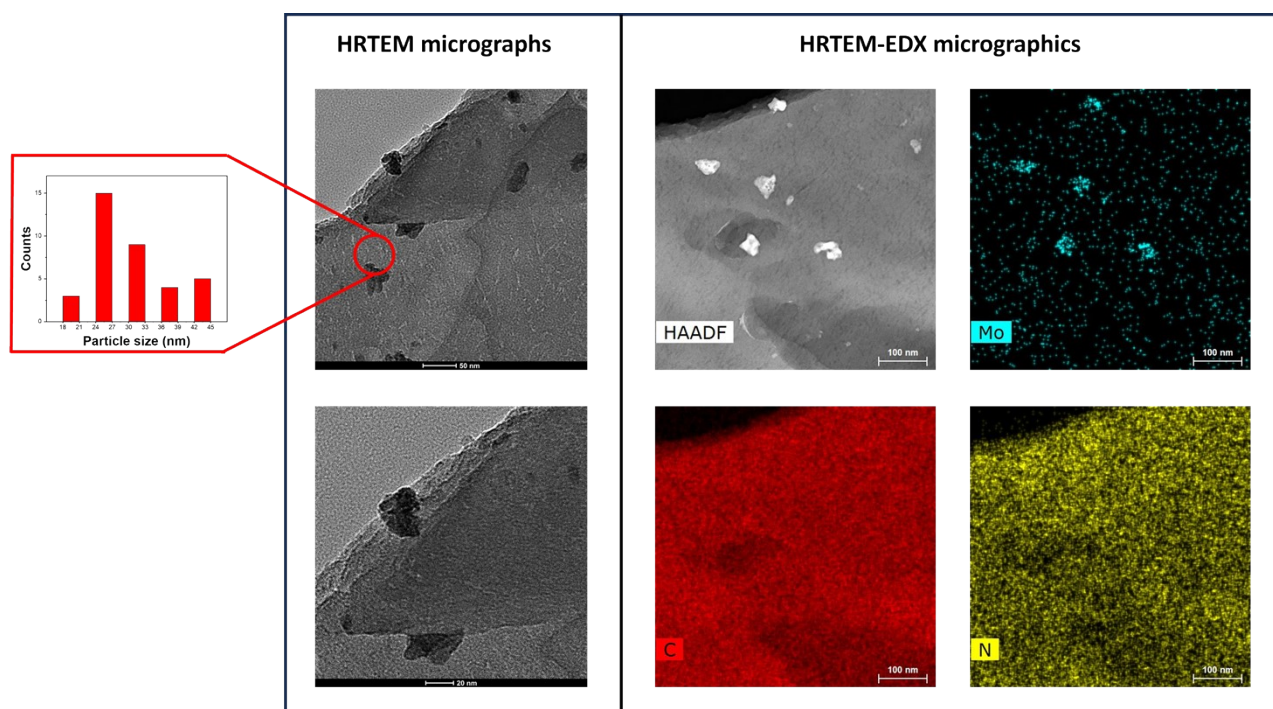


Figure S3: *on the left: HRTEM micrographs of the Mo(5%)-N/C sample; on the right: HRTEM in STEM mode-EDX micrographics of the Mo(5%)-N/C sample.*

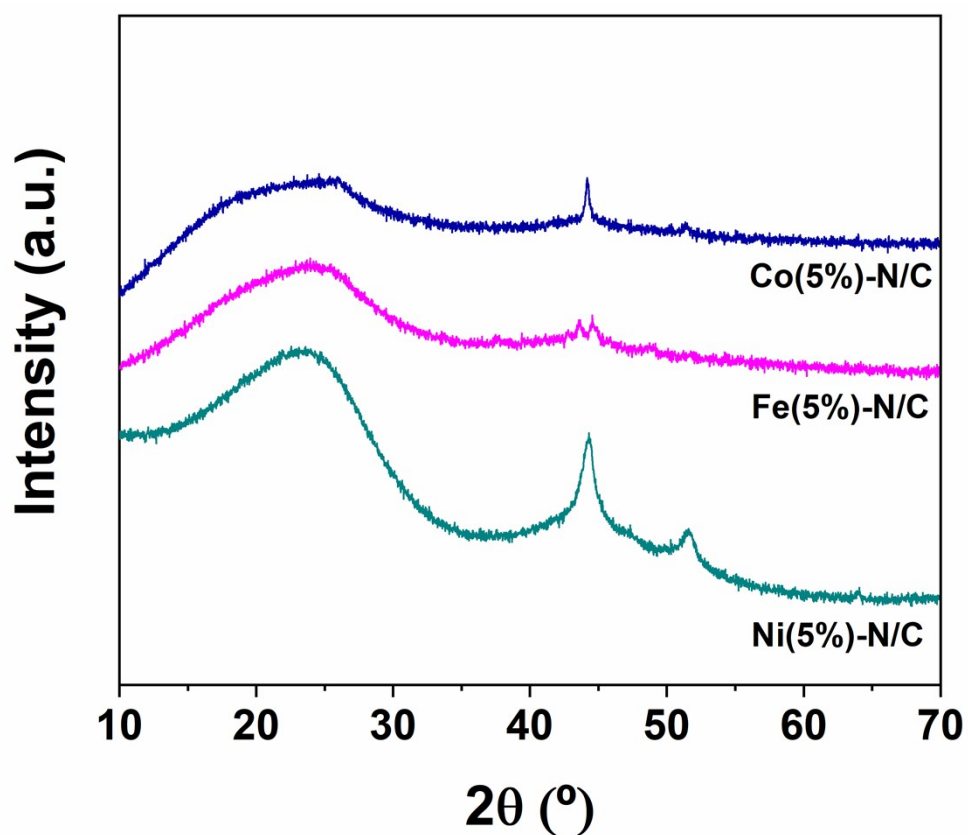


Figure S4. XRD patterns of the Ni(5%)-N/C, Fe(5%)-N/C and Co(5%)-N/C catalytic materials.

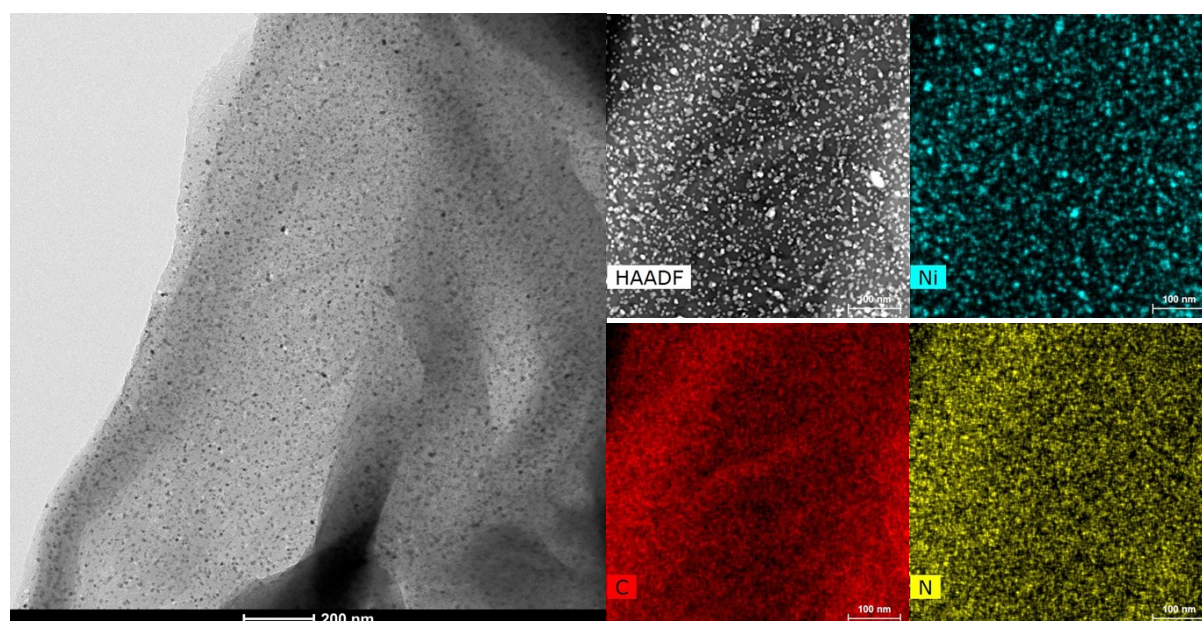


Figure S5. HRTEM(STEM)-EDX images of the Ni(5%)-N/C catalytic material.

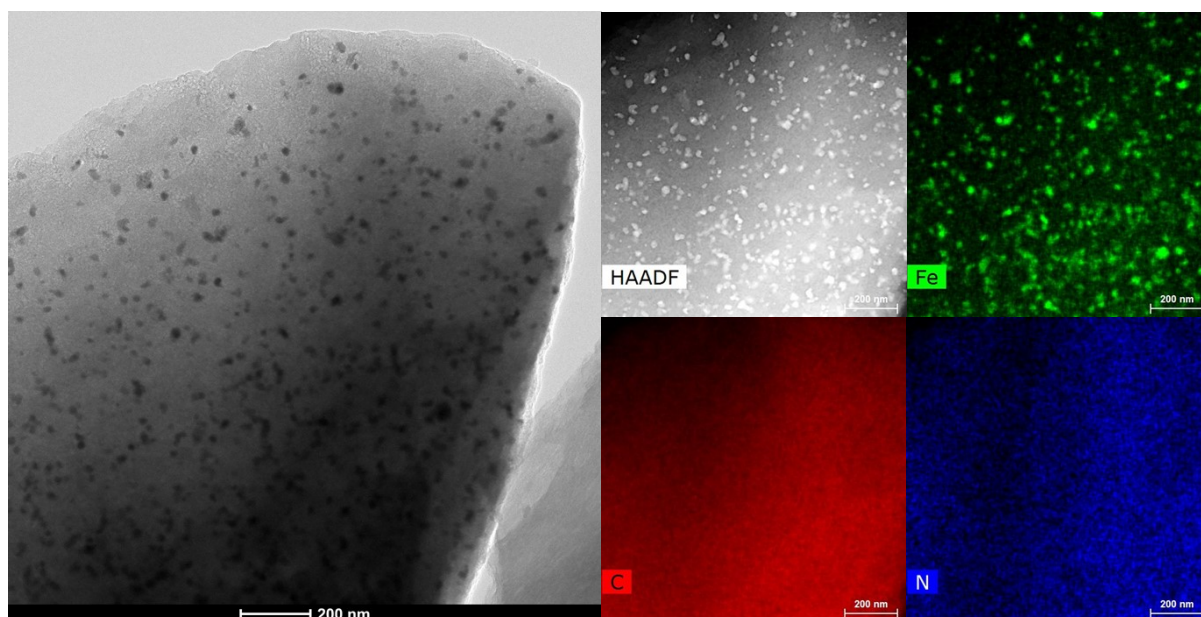


Figure S6. HRTEM(STEM)-EDX images of the Fe(5%)-N/C catalytic material.

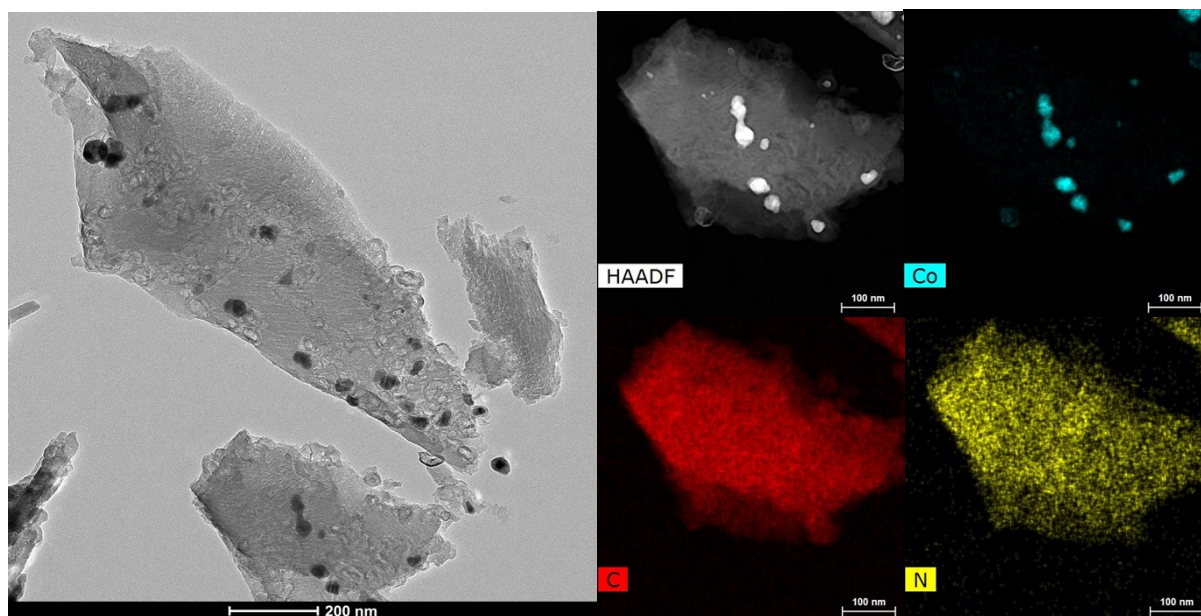


Figure S7. HRTEM(STEM)-EDX images of the Co(5%)-N/C catalytic material.

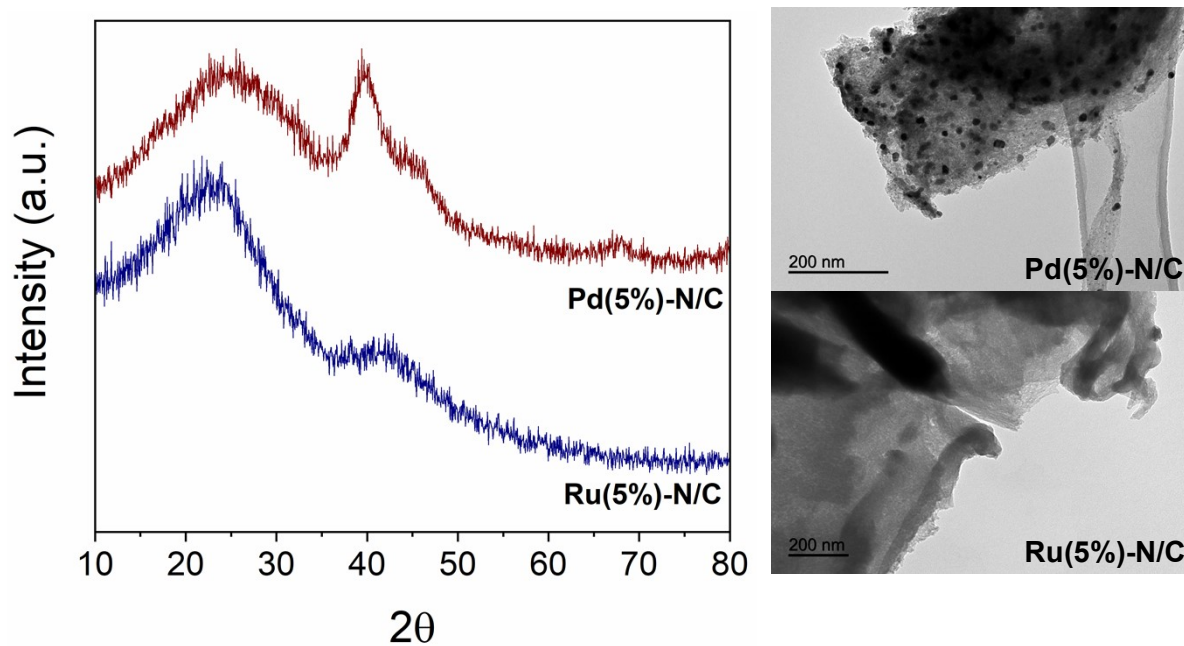


Figure S8. XRD patterns and HRTEM micrographs of the Pd(5%)-N/C and Ru(5%)-N/C catalytic materials.

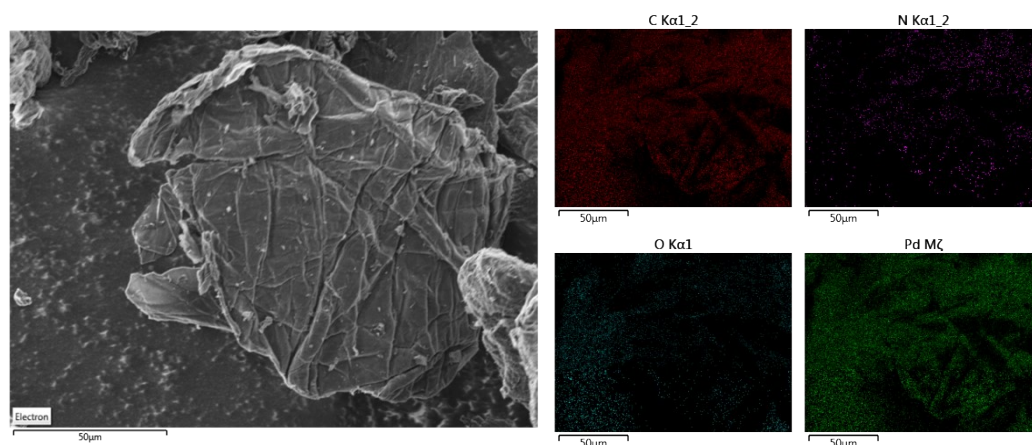


Figure S9. SEM-mapping micrographs of the Pd(5%)-N/C catalytic material.

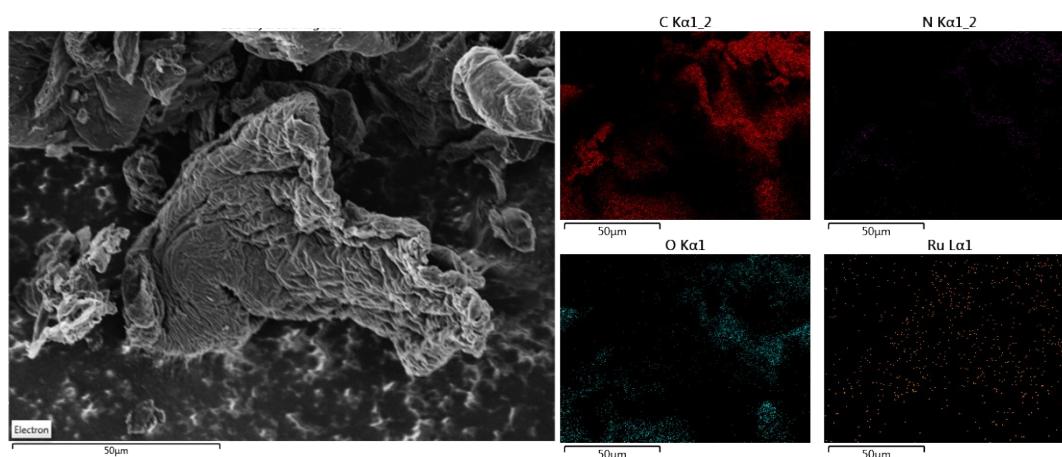


Figure S10. SEM-mapping micrographs of the Ru(5%)-N/C catalytic material.

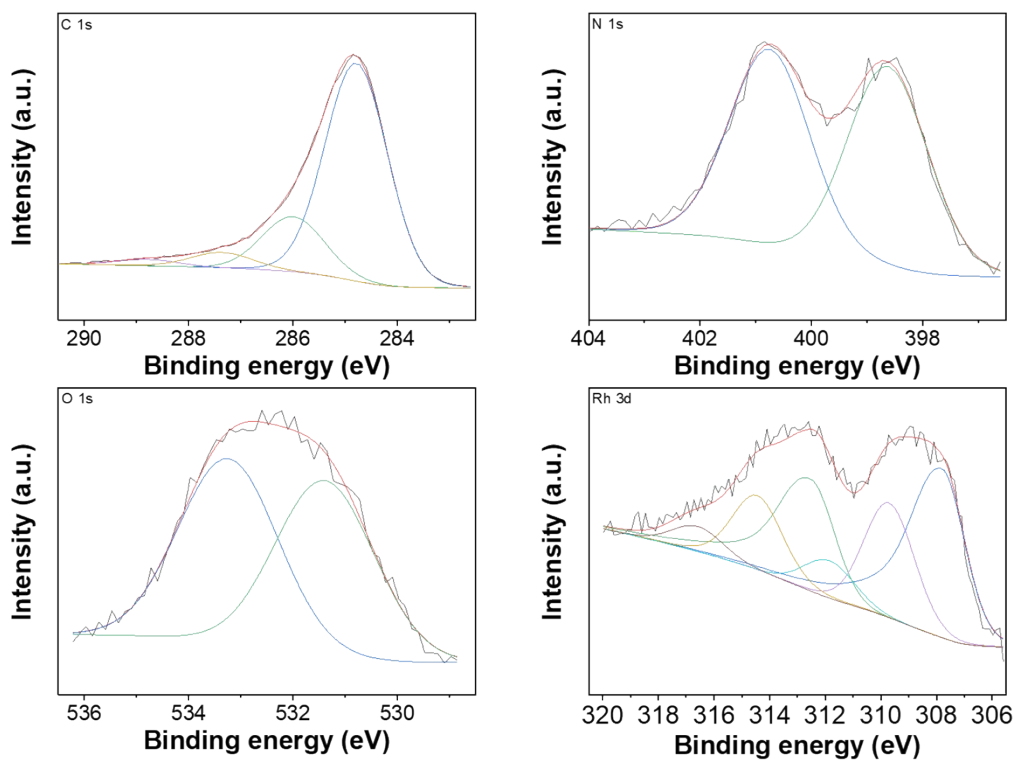


Figure S11: XPS spectra of the Rh(1%)-N/C, including C 1s, N 1s, O 1s and Rh 3d regions.

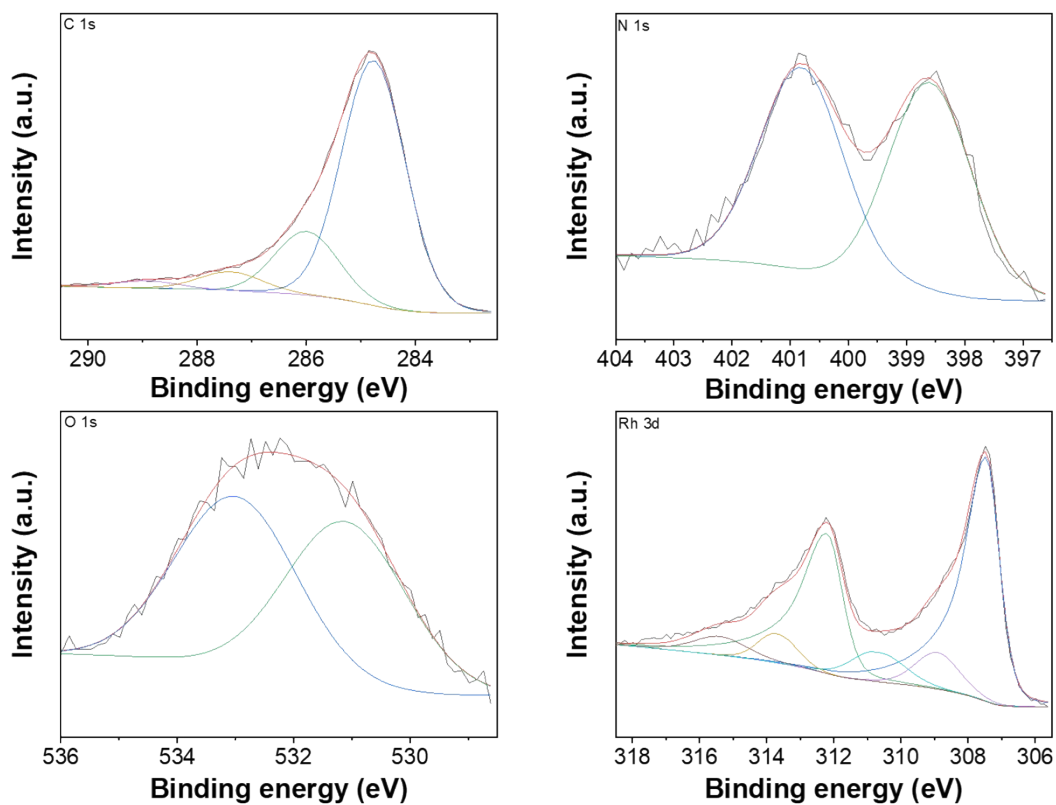


Figure S12: XPS spectra of the Rh(3%)-N/C, including C 1s, N 1s, O 1s and Rh 3d regions.

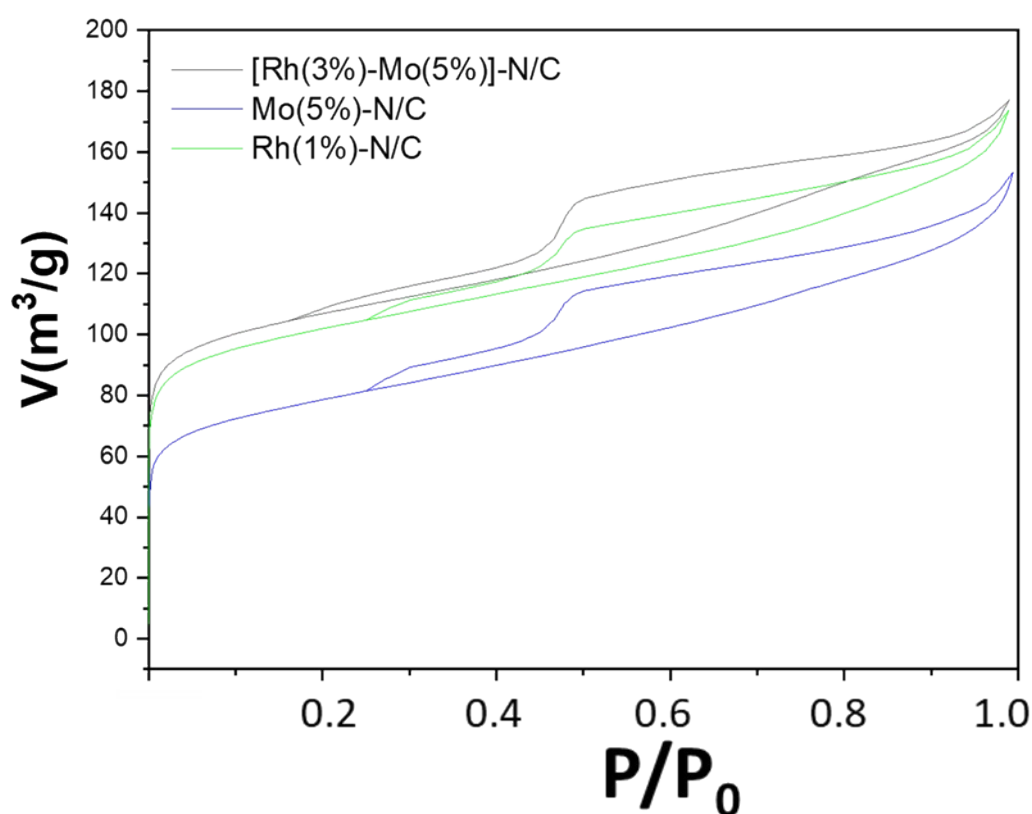


Figure S13: N_2 -physorption isotherms at -196°C of the prepared bimetallic $[\text{Rh}(3\%)\text{-Mo}(5\%)]\text{-N/C}$ sample, and its comparison with the isotherms of the $\text{Rh}(1\%)\text{-N/C}$, and $\text{Mo}(5\%)\text{-N/C}$ samples.

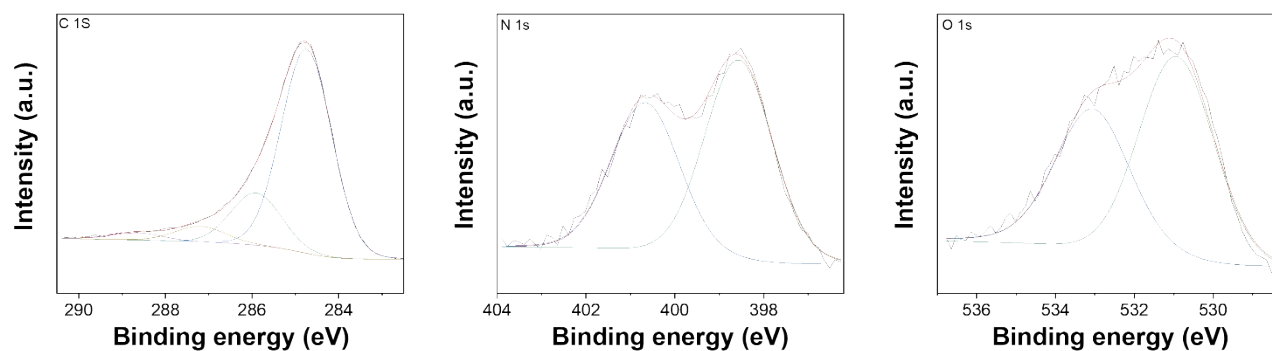


Figure S14: XPS spectra of the $[\text{Rh}(3\%)\text{-Mo}(5\%)]\text{-N/C}$ sample, including C 1s, N 1s and O 1s regions.

Table S2. XPS binding energies and quantification analysis in the N 1s XPS region, and the corresponding Rh-N contribution in the Rh $3d_{5/2}$ XPS region.

Entry	Sample	N_{pl} 1s/eV	N_p 1s/eV	N_{il} 1s/	N_p 1s/eV	N_{pl} %	N_p %	N_p/N_{pl}	Rh-N %
				FWHM	FWHM				
1	Rh(1%)-N/C	398.6	400.7	659	648	50.4	49.6	0.98	5.9
2	Rh(3%)-N/	398.6	400.8	456	437	51.0	48.9	0.96	7.0
3	Rh(5%)-N/C	398.69	400.5	699	622	52.5	47.1	0.89	7.66

A decrease in the pyridinic-pyrrolic nitrogen ratio was observed, likely attributable to the higher metal content in the catalytic samples and, thus, a higher number of metal-nitrogen bonds. Also, the Rh-N signal (ca. 310 eV) in the Rh $3d_{5/2}$ increased accordingly.

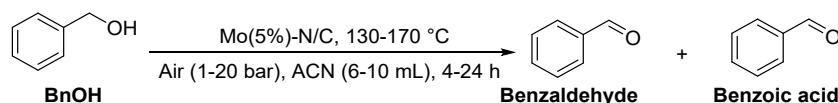
Numerous studies have explored the interactions of nitrogen sites with metallic entities, employing various methodologies, including computational approaches.⁵¹ In a typical N-doped carbon based material, different types of nitrogen groups have been defined as pyridinic, pyrrolic and graphitic groups.¹ Pyridinic group is a type of nitrogen that is doubly coordinated and usually found on the edge or within vacancies of graphitic domains. It contributes a single p-electron to the π system, and its lone pair gives it a basic character. On the other hand, pyrrole nitrogen is a three-fold coordinated nitrogen atom located in a pentagonal ring. When substituted in graphene, pyrrole acts as an electron localizer and behaves as a 2-position nucleophile. The presence of nitrogen favors the deposition of metal nanoparticles. However, the electron-rich characteristics of pyrrolic nitrogen prevent the formation of a direct nitrogen-metal bond due to the high electrostatic repulsion with metal nanoparticles. On the contrary, pyridinic nitrogen shares only one electron with the π system of the support, allowing direct coordination of the metal nanoparticles. This is facilitated by the σ -donation of nitrogen to the metal and a possible back-donation of the metal to the now free π^* orbital of the support. In this way, pyridinic nitrogen can not only promote proper dispersion of active sites but also enhances the stability of catalytic systems by acting as an anchoring site to prevent metal leaching.

Without a doubt, this topic requires more extensive research to understand the intimate nature of metal-nitrogen interactions. This area is currently a focal point of research within our group, specifically in cases where the support material could potentially play a significant role, not only as a support but also in the catalytic reaction itself.

S1. Mao, S.; Wang, C.; Wang, Y. The Chemical Nature of N Doping on N Doped Carbon Supported Noble Metal Catalysts. *J Catal* 2019, 375, 456–465. <https://doi.org/10.1016/j.jcat.2019.06.039>.

The parametric analysis of the oxidation of BnOH using Mo(5%)-N/C as a catalyst.

The oxidation of BnOH was investigated under the conditions summarized in Scheme SX



Scheme S1. Benzyl alcohol oxidation reaction.

Results of Fig. S15 A-D illustrates the effect of temperature, pressure, volume of solvent, and time, respectively, at a constant catalyst amount (50 mg), while Fig. S16 shows the effect of the amount of catalyst during reactions run at 170 °C, 1 atm, 18 h, and V of ACN of 10 mL. A blank experiment (130 °C, 20 bar, 24 h; not reported in the figures) afforded a negligible conversion of ca 3%.

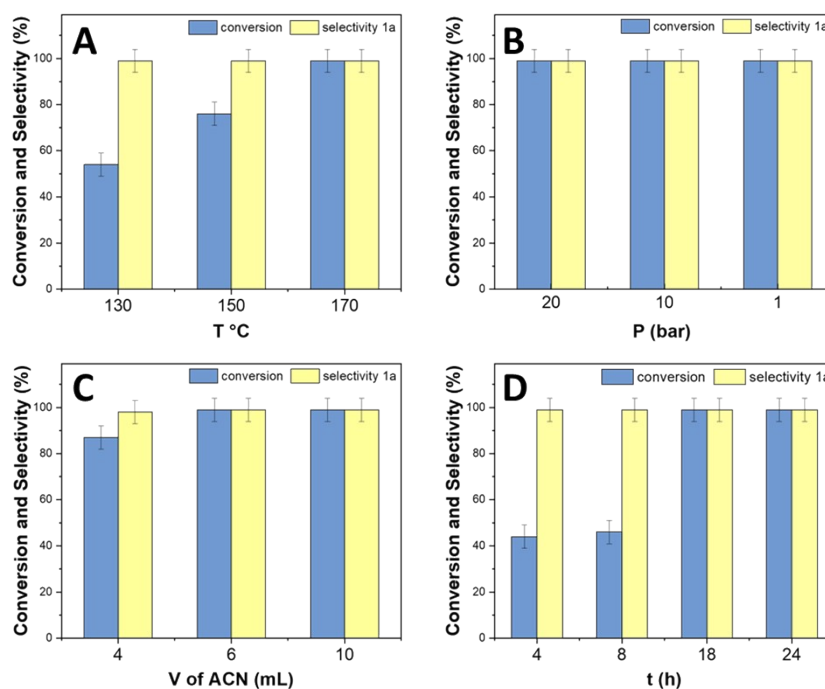


Figure S15. Parametric analysis of the oxidation of BnOH using the Mo(5%)-N/C as a catalyst (50 mg). Benzaldehyde: **1a**; Benzoic acid: **1b**. Effect of: **A**) temperature, **B**) pressure, **C**) volume of solvent, **D**) reaction time. Other conditions: **A**) 20 bar, 24 h, $V_{ACN} = 10$ mL; **B**) 170 °C, 24 h, $V_{ACN} = 10$ mL; **C**) 170 °C, 1 atm, 24 h; **D**) 170 °C, 1 atm, $V_{ACN} = 10$ mL.

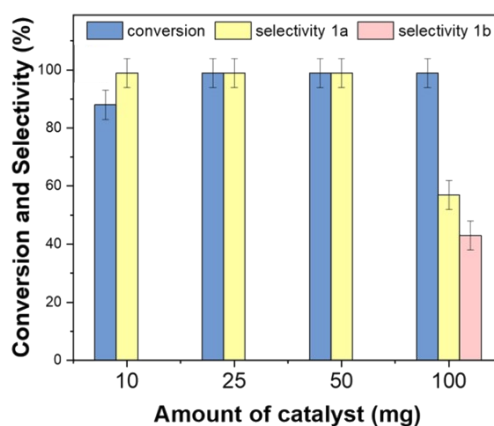


Figure S16. Parametric analysis of the oxidation of BnOH using the Mo(5%)-N/C as a catalyst. Benzaldehyde: **1a**; Benzoic acid: **1b**. Effect of catalyst amount. Other conditions: 170 °C, 18 h, $V_{ACN} = 10$ mL

Temperature. The best outcome was achieved at 170 °C for 24 h, with conversion and selectivity exceeding 99% (**Fig. S15A**). At 130 and 150 °C, a complete selectivity to benzaldehyde was still allowed, but alcohol conversion was only 52% and 75%, respectively. The analysis was therefore continued at 170 °C.

Pressure. The influence of the pressure was investigated from ambient up to 20 bar (**Fig. S15B**). Notably, conversion and yield remained consistently above 99% even without pressurizing the autoclave.

Solvent volume. Tests carried out for 24 h at 170 °C and 1 atm, did not show significant changes in the reaction outcome when the amount of ACN was reduced from 10 mL to 6 mL (**Fig. S15C**). Though, a further decrease to 4 mL resulted in a drop in conversion from $\geq 99\%$ to 87%. This result was apparently inconsistent because increasing the concentration (by reducing the solvent) was expected to induce an increase in reaction rate. A hypothesis for this discrepancy considered the drop in solubility of the oxidant (oxygen) in ACN:²⁸ the lower the amount of the solvent, the lower the oxygen available for the reaction, the lower the conversion. The study was then continued using the maximum tested amount of ACN (10 mL).

Reaction time. Experiments were run at 170 °C, 1 atm, $V_{ACN} = 10$ mL by varying the duration from 24 to 4 hours.

(Fig. S15D). It was proved that the reaction was quantitative and with full selectivity to benzaldehyde after 18 h, while shorter reaction times from 4 to 6 h resulted in significantly lower conversion, around 45%.

The catalyst amount. At 170 °C, 1 atm, 18 h, $V_{\text{ACN}} = 10$ mL, tests demonstrated that halving the quantity of Mo(5%)-N/C, from 50 to 25 mg, had no effect on either the conversion or the benzaldehyde selectivity, which both remained above 99% (Fig. S16). By contrast, a further decrease to 10 mg brought about a decrease in conversion to 88%, while an increase to 100 mg resulted in a drop in selectivity to 56% due to the formation of benzoic acid from the overoxidation of BnOH.

The parametric analysis of the reductive amination of benzaldehyde using Ru(5%)-N/C as a catalyst.

A parametric analysis of the reductive amination of benzaldehyde was carried out by varying: i) the amount of catalyst, from 25 to 75 mg; ii) the temperature, from 60 to 120 °C; ii) the hydrogen pressure, from 10 to 50 bar; iii) the reaction time, from 4 to 24 h, and the volume of acetonitrile (ACN), from 6 to 10 mL. Results are reported in Figure S17.

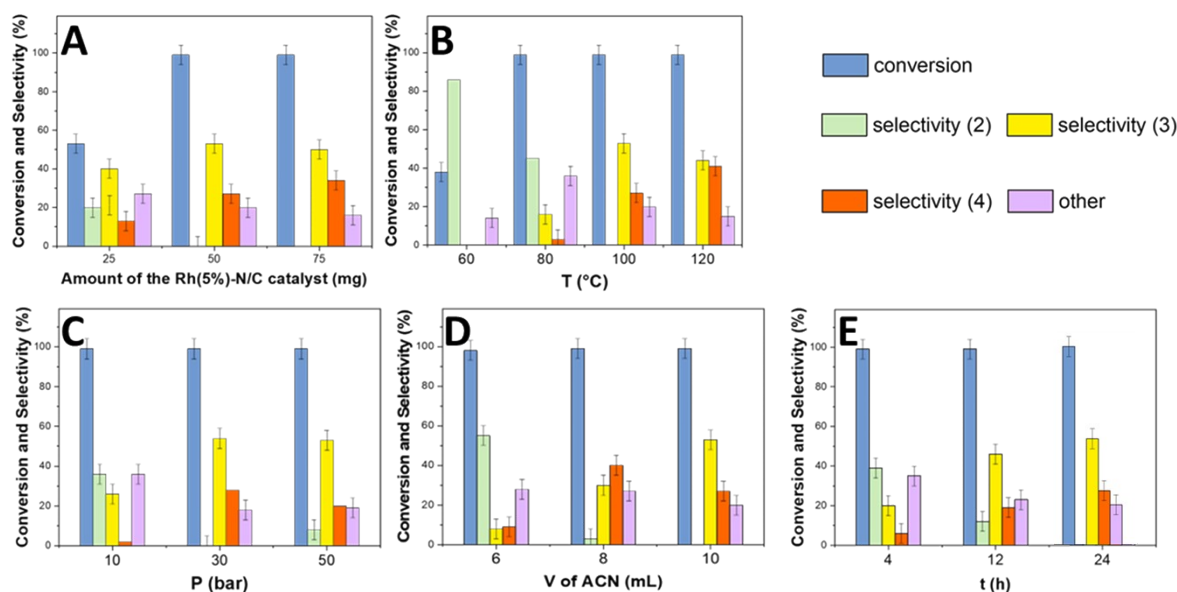


Figure S17. Parametric analysis of the reductive amination of benzaldehyde with acetonitrile catalyzed by [Rh(5%)-N/C]. Other conditions: **A**) 100 °C, 30 bar, 24 h, $V_{\text{ACN}} = 10$ mL; **B**) 30 bar, 50 mg, 24 h, $V_{\text{ACN}} = 10$ mL; **C**) 100 °C, 50 mg, 24 h, $V_{\text{ACN}} = 10$ mL; **D**) 100 °C, 30 bar, 50 mg, 24 h; **E**) 100 °C, 30 bar, 50 mg, $V_{\text{ACN}} = 10$ mL.

The effect of *catalyst amount* was initially investigated as displayed in Figure S17A. An unsatisfactory outcome was attained with the lowest tested quantity of catalyst, which resulted in a moderate conversion (53%) and no significant preference towards any of the observed products. In contrast, doubling of Rh(5%)-N/C amount (50 mg) not only allowed complete conversion, but also improved the formation of product **3** to 53%. The overall selectivity of the reductive amination became 53% (total **2+3**; compare Figure S17) without considering compound **4** (27%) because of the reasons explained in Scheme 5. However, a higher amount of catalyst (75 mg) was not beneficial for the selectivity to the desired secondary amine. Further experiments were then designed using 50 mg of Rh(5%)-N/C.

The influence of *temperature* was also explored as shown in Figure S17B. The most favorable temperature to achieve the secondary amine **3** was 100 °C, which was then selected to continue the study. This confirmed the results of Figure 14. Interestingly, at 60 °C, an exceptionally high selectivity (86%) toward imine **2** was observed, yet the conversion was too low (38%) for any practical use in synthesis.

The H_2 Pressure was subsequently investigated (Figure S17C). Amine **3** was obtained with a comparable selectivity of 53% and 51%, at 30 and 50 bar, respectively. Consequently, the lower and most economical pressure (30 bar) was selected for further experiments. Additional tests were carried out to explore the combined effect of pressure and temperature. Particularly, the reaction was carried out at 80 °C by changing the pressure from 10 to 50 bar (other conditions: Rh(5%)-N/C=50 mg and $V_{\text{ACN}} = 10$ mL). The results are reported in Figure S18.

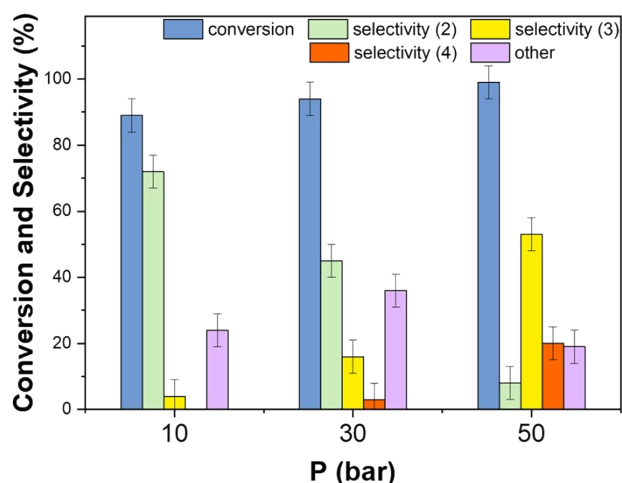
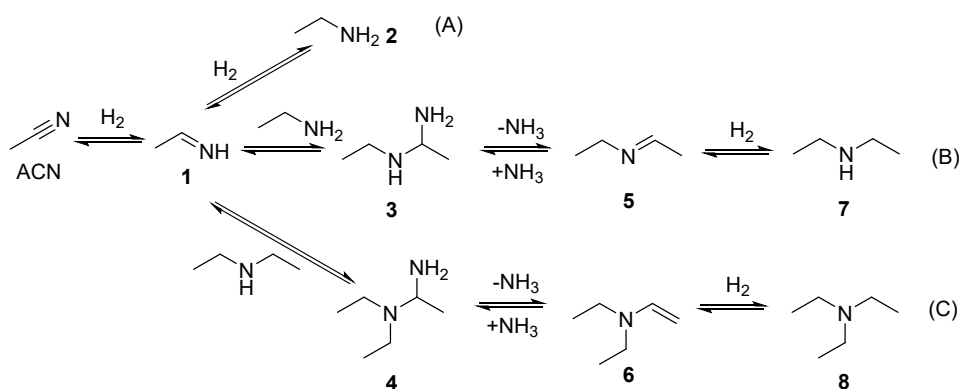


Figure S18. Effect of pressure on the reductive amination of benzaldehyde with acetonitrile carried out 80 °C. Other conditions: Rh(5%)-N/C=50 mg; V_{ACN} =10 mL.

It was observed that the same selectivity (53-54%) toward **3** was achieved at 80 °C/50 bar and 100 °C/30 bar (compare Figure 15C). On the other hand, lower T and P tend to favor the formation of imine **2** (up to 72% at 10 bar and 89% conversion) and “others”. This result was consistent with the fact that the kinetics of reductive amination took advantage either from the temperature or from the availability/solubility of gaseous hydrogen in the liquid phase which increased with pressure. It was finally decided to operate at 100 °C/30 bar because a higher pressure was both a greater safety hazard and a higher cost compared to a temperature decrease from 100 to 80 °C.

The volume of ACN and the reaction time was finally studied (Figure 15D-E). This study highlighted that the selectivity towards amine **3** was progressively improved to 52-54% by increasing solvent volume and reaction time up to 10 mL and 24 h, respectively. Interestingly, two facts emerged: i) at the lowest investigated volume of ACN (6 mL), the reaction was quantitative but a consistent formation of the imine **2** (55%) was achieved (Figure 15D). This suggests that a larger amount of solvent favored the reduction **2**→**3** by plausibly dissolving more hydrogen in the liquid phase and making it available for the hydrogenation processes; ii) a quantitative conversion (>99%) was achieved even after 4 hours, but imine **2** was the predominant product (55%), *i.e.* the process was not long enough to allow the hydrogenation of **2** (Figure 15D). However, by prolonging the reaction to 12 and 24 h, compounds **2** and **3** decreased and increased, respectively, to almost the same amount, meaning that the former was gradually transformed into the latter. Simultaneously, the formation of “others” diminished in favor of product **4** which indicated that the latter (tertiary amine **4**) could be sourced by “others”. This was suggested also by the trends of Figures 15A-D where in general, if the reaction was allowed to proceed by increasing T, P, and the solvent volume, the lower the amount “others”, the higher the amount of the amine **4**.

1. Reaction pathway of the reduction of ACN



Scheme S2: reaction pathway of the reduction of ACN; **1**: ethanimine; **2**: ethyl amine; **3**: N-ethyl aminal; **4**: N-diethyl aminal; **5**: ethylethanamine; **6**: diethylethanamine; **7**: diethylamine; **8**: triethylamine.⁵⁰

Table S3. Comparative analysis of reductive amination reactions in literature.

Entry	Carbonyl/nitrogen containing substrates	Catalyst	Conditions T(°C)/p(bar)/t(h)	Conversion (%)	Selectivity (%) [*]	Ref
1	Benzaldehyde/Aniline	CuAlO _x	120 °C, 20 bar, 3 h	96	>99	S2
2	Benzaldehyde/Aniline	[(κ ⁴ -{1,2-C ₆ H ₄ (N=CH-C ₆ H ₄ O) ₂ }Pd]	60 °C, 12 h ^{**}	>99	90	S3
3	Levulinic acid/ACN	Ru/TiO ₂	90 °C, 50 bar, 0.3 mL min ⁻¹	79	85	S4
4	Furfural/ACN	TiO ₂ -Rh1%	100 °C, 20 bar, 2 h	>99	76	S5
5	Furfural/ACN	5 wt% Pt/C	100 °C, 20 bar, 2 h	>99	42	S5
6	Furfural/ACN	5 wt% Pd/C	100 °C, 20 bar, 2 h	>99	25	S5
7	Furfural/ACN	5 wt% Ru/C	100 °C, 20 bar, 2 h	71	-	S5
8	Benzaldehyde/NH ₃	Rh/COF2	90 °C, 20 bar, 15 h	>99	95	S6
9	Benzaldehyde/NH ₃	Rh/COF	90 °C, 20 bar, 15 h	>99	76	S7
10	Benzaldehyde/ACN	Pt/P25	90 °C, 50 bar, 0.3 mL min ⁻¹	>99	60%	S8
11	Benzaldehyde/ACN	Ru(5%)-N/C	100 °C, 50 bar, 24 h	>99	- ^a	This work
12	Benzaldehyde/ACN	Pd(3%)-N/C	100 °C, 50 bar, 24 h	>99	- ^a	This work
13	Benzaldehyde/ACN	MIX1	100 °C, 30 bar, 24 h	>99	66 ^b	This work
14	Benzaldehyde/ACN	MIX2	100 °C, 50 bar, 24 h	>99	60 ^c	This work

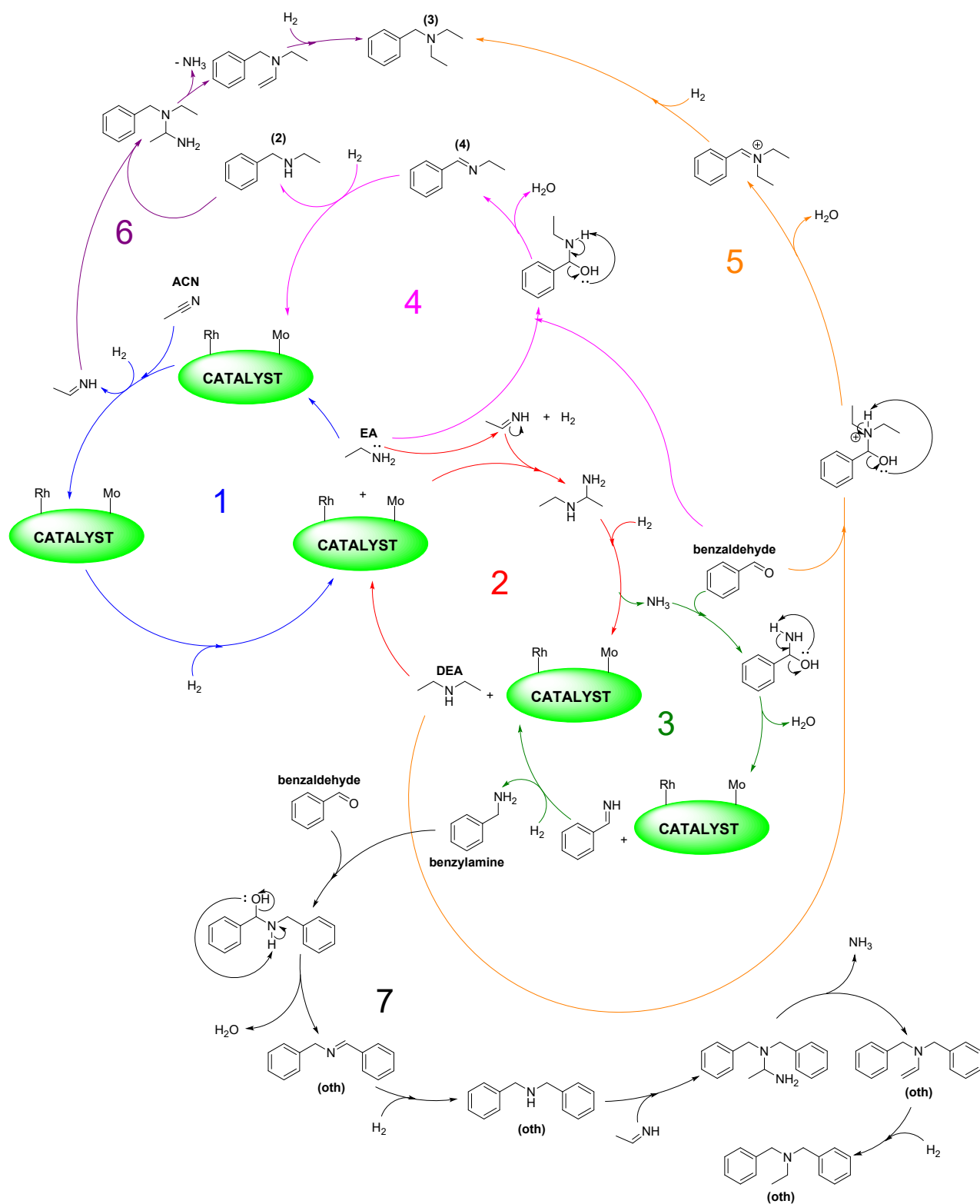
^{*}Products of reductive amination; ^a only oxidation products observed; ^b secondary amine; ^c tertiary amine

^{**}HBpin as reducing agent

- S2. Nuzhdin, A. L., Bukhtiyarova, M. V., & Bukhtiyarova, G. A. (2020). Cu-Al mixed oxide derived from layered double hydroxide as an efficient catalyst for continuous-flow reductive amination of aromatic aldehydes. *Journal of Chemical Technology & Biotechnology*, 95(12), 3292-3299.
- S3. Mahato, S., Rawal, P., Devadkar, A. K., Joshi, M., Choudhury, A. R., Biswas, B., ... & Panda, T. K. (2022). Hydroboration and reductive amination of ketones and aldehydes with HBpin by a bench stable Pd (II)-catalyst. *Organic & Biomolecular Chemistry*, 20(5), 1103-1111.
- S4. Rodriguez-Padron, D., Puente-Santiago, A. R., Balu, A. M., Romero, A. A., Munoz-Batista, M. J., & Luque, R. (2018). Benign-by-design orange peel-templated nanocatalysts for continuous flow conversion of levulinic acid to N-heterocycles. *ACS Sustainable Chemistry & Engineering*, 6(12), 16637-16644.
- S5. Polidoro, D., Espro, C., Lazaro, N., Trentin, O., Perosa, A., Osman, S. M., ... & Selva, M. (2023). Catalytic screening of the cascade reductive amination reaction of furfural and acetonitrile. *Catalysis Today*, 423, 113890.

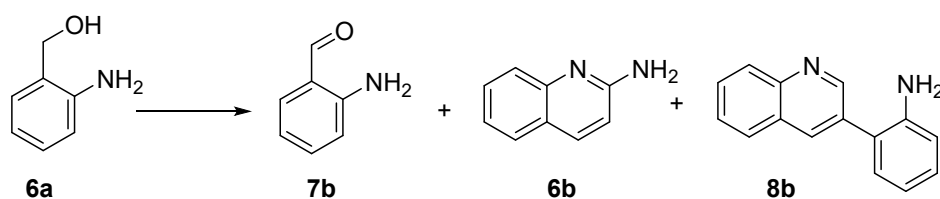
- S6. Wang, N., Liu, J., Tang, L., Wei, X., Wang, C., Li, X., & Ma, L. (2021). Facile synthesis of Rh anchored uniform spherical COF for one-pot tandem reductive amination of aldehydes to secondary Imines. *ACS Applied Materials & Interfaces*, 13(21), 24966-24975.
- S7. Wang, N., Liu, J., Li, X., & Ma, L. (2023). Selective control in the reductive amination of benzaldehyde towards corresponding amines over COF supported Pt, Pd, and Rh catalysts. *Catalysis Communications*, 175, 106620.
- S8. Altuğ, C., Muñoz-Batista, M. J., Rodríguez-Padrón, D., Balu, A. M., Romero, A. A., & Luque, R. (2019). Continuous flow synthesis of amines from the cascade reactions of nitriles and carbonyl-containing compounds promoted by Pt-modified titania catalysts. *Green Chemistry*, 21(2), 300-306.

3. Tandem reaction pathway



Scheme S3: Schematic representation of the processes that lead to the formation of all observed species during the reductive amination of Benzaldehyde in ACN.

4. Substrate scope: 2-aminobenzyl alcohol



Scheme S4. The reaction of 2-aminobenzyl alcohol (**6a**) under oxidative conditions (170 °C; 1 atm, 18 h, V_{ACN} =10 mL). 2-aminobenzaldehyde iminoquinoline (**6b**), and 2-(3-quinolinyl) aniline (**8b**) were the observed products.

Results are reported in Fig. 40.

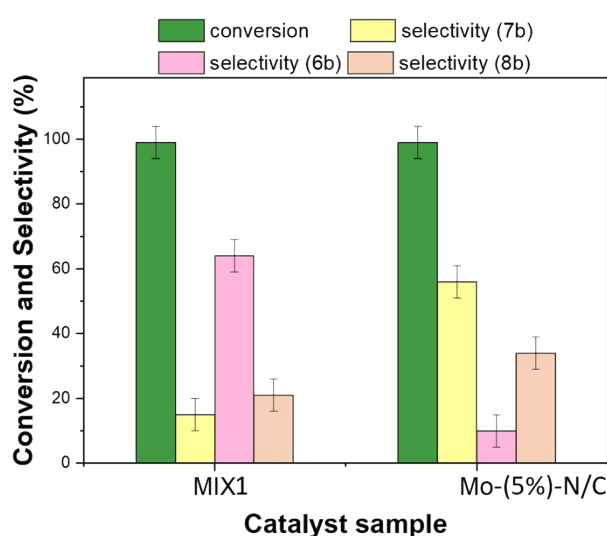


Figure S19. The reaction of **6a** under oxidative conditions. Left: in the presence of MIX1 (mechanical mixture of Rh(5%)-N/C and Mo(5%)-N/C; right: in the presence of Mo(5%)-N/C alone.

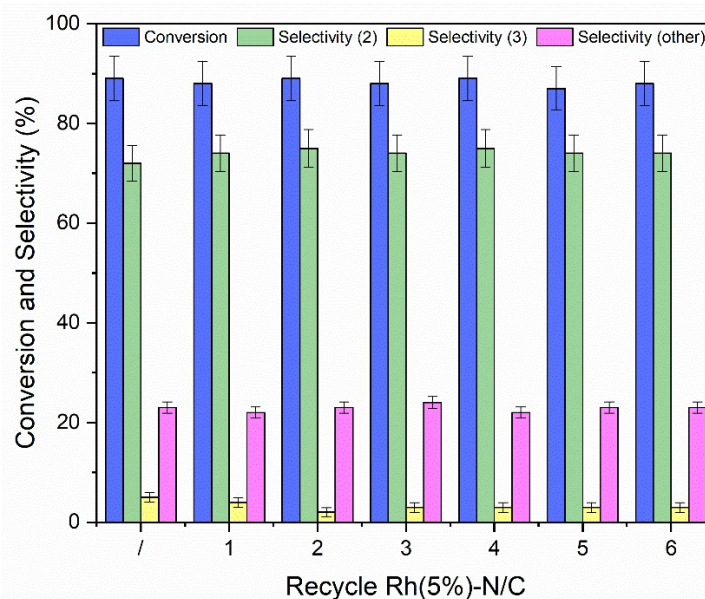
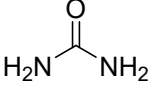


Figure S20. Catalyst recycle. Rh(5%)-N/C recycles in the reductive amination of benzaldehyde with ACN (10 mL) carried out at 80 °C, 10 bar of H₂, and 24 h.

5. Mechanochemical assisted reaction

Table S4 summarizes the conditions used for the mechanochemical assisted reaction.

Table S4: reaction conditions for the mechanochemical tests, *2a: Vanillic alcohol.

Catalyst sample (amount)	2a amount	Oxidizing agent (amount)	T °C	rpm	t h
Mo(5%)-N/C (100 mg)	2 g (18 mmol)	H ₂ O ₂ hydrogen peroxide (1.2 eq)	80	100	1
Mo(5%)-N/C (100 mg)	2 g (18 mmol)	 · H ₂ O ₂ urea peroxide (2.5 eq)	80	100	1
Mo(5%)-N/C (100 mg)	2 g (18 mmol)	Air (8 mL/min)	80	100	1

6. Formulas for the calculation of green metrics

Table S5: formulas for the calculation of green metrics.⁵¹

$$\text{Percentage yield} = \frac{\text{moles of product}}{\text{moles of limiting reactant}} \times 100$$

$$\text{Percentage conversion} = 100 - \left(\frac{\text{final mass of limiting reactant}}{\text{initial mass of limiting reactant}} \times 100 \right)$$

$$\text{Percentage selectivity} = \frac{\% \text{yield}}{\% \text{conversion}} \times 100$$

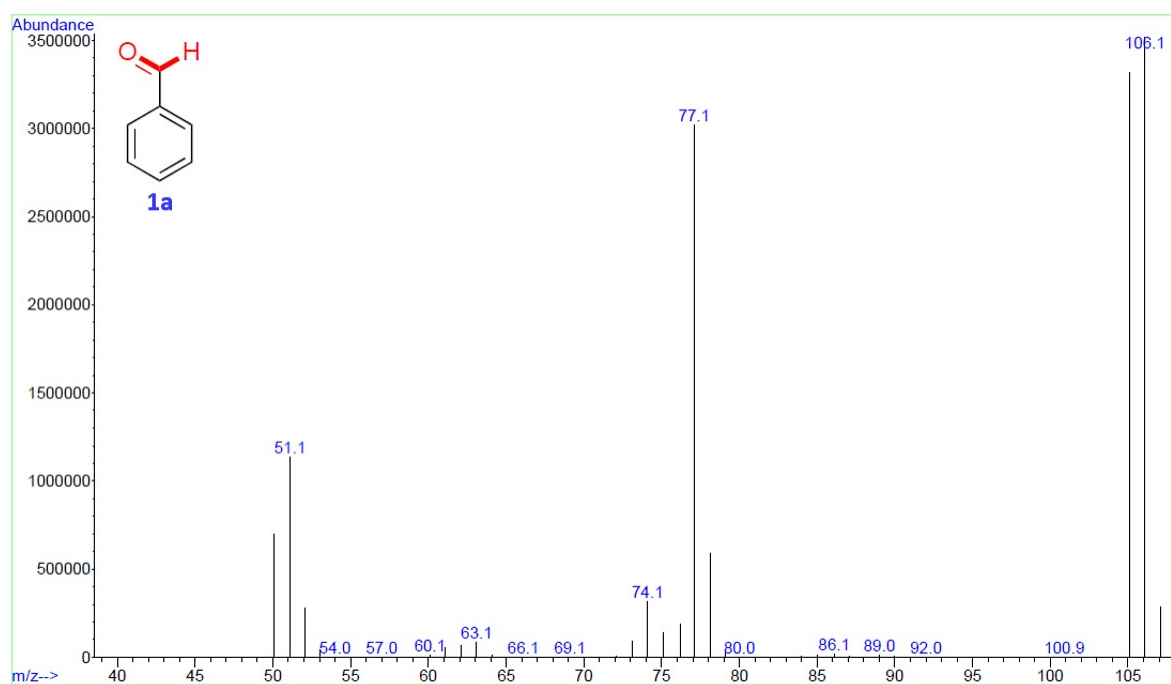
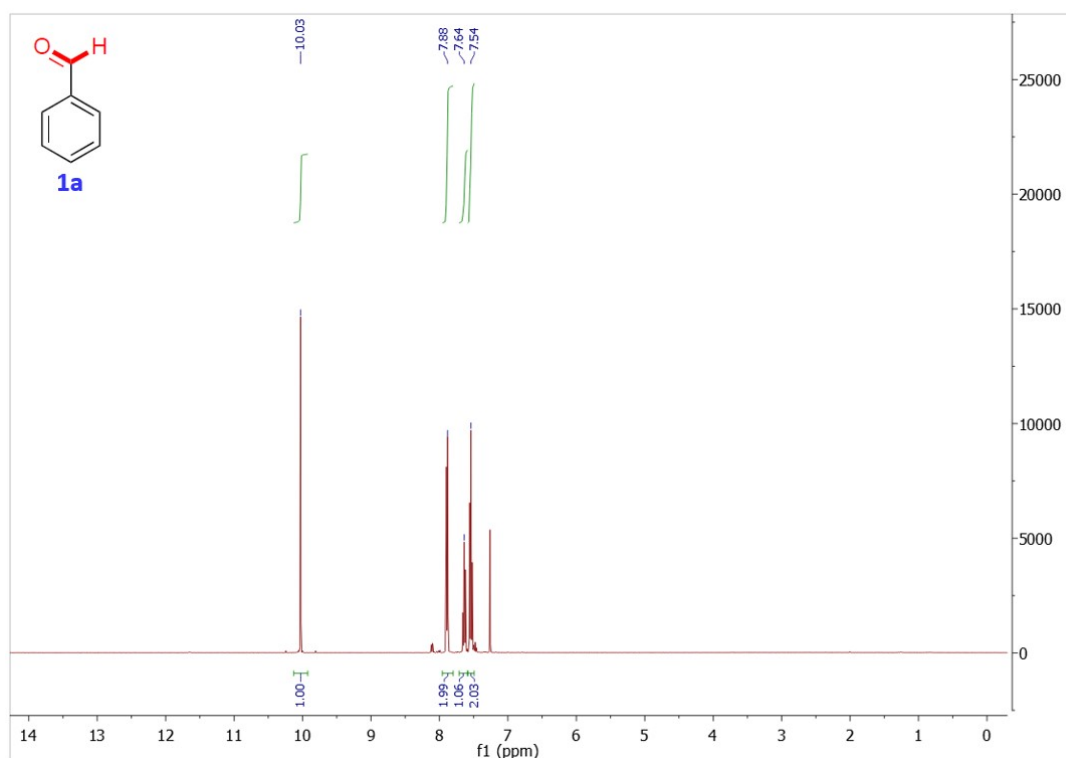
$$AE = \frac{\text{molecular weight of products}}{\text{total molecular weight of reactants}} \times 100$$

$$RME = \frac{\text{mass of isolated product}}{\text{total mass of reactants}} \times 100$$

$$OE(\text{optimum efficiency}) = \frac{RME}{AE} \times 100$$

$$MI (\text{Mass Intensity}) = \frac{\text{total mass in a process step}}{\text{mass of product}}$$

7. Products characterization

Figure S21. Mass Spectrum of **1a** (EI, 70 eV).Figure S22. ¹H NMR of **1a**. ¹H NMR (400 MHz, 298 K, CDCl₃) δ 10.03 (s, 1H), 7.88 (d, 2H), 7.64 (t, 1H), 7.54 (t, 2H).

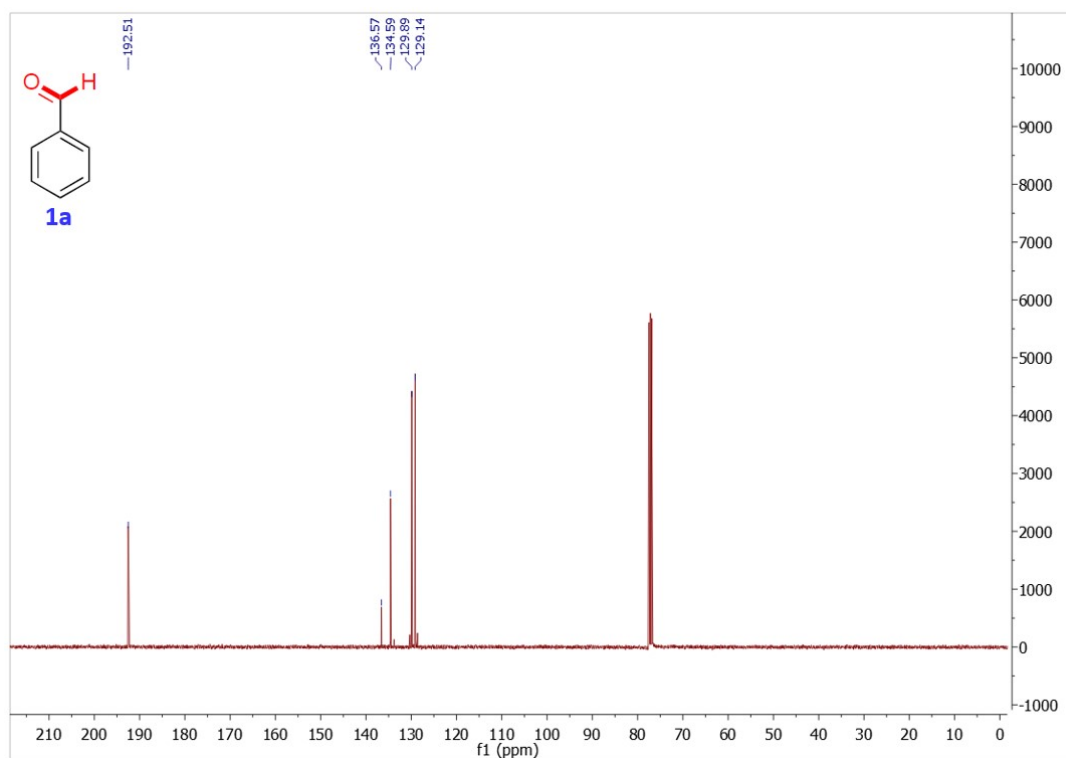


Figure S23. ¹³C NMR of **1a**. ¹³C NMR (101 MHz, 298 K, CDCl₃) δ 192.51, 136.57, 134.59, 129.89, 129.14.

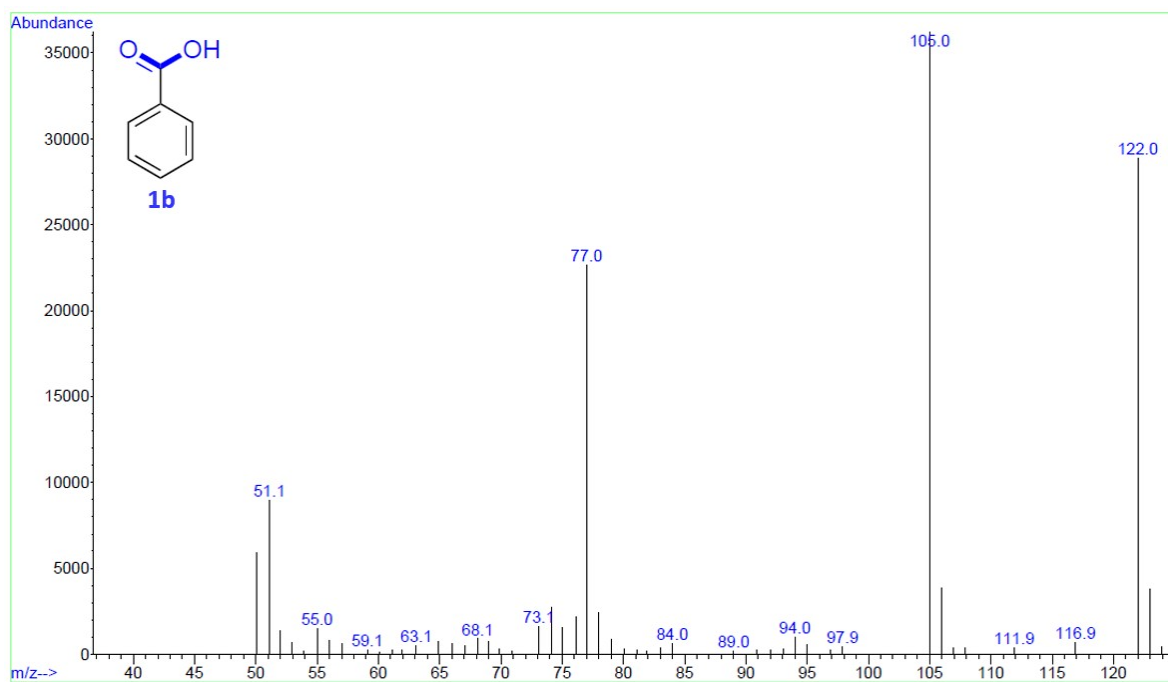


Figure S24. Mass Spectrum of **1b** (EI, 70 eV).

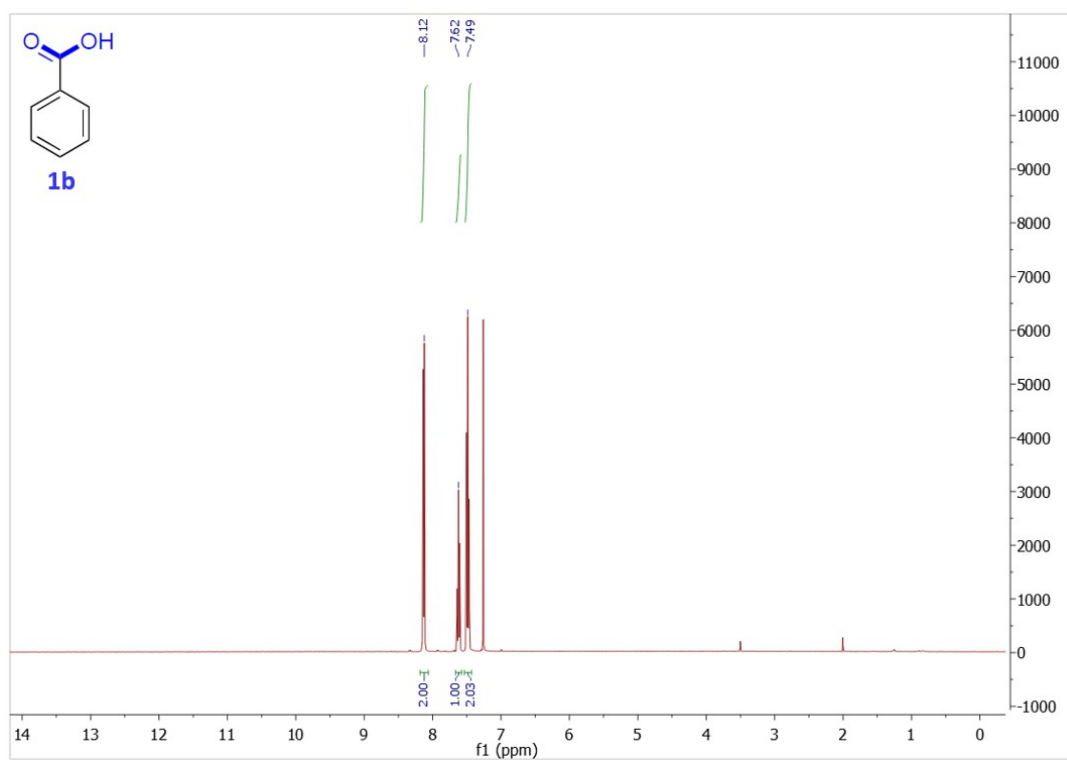


Figure S25. ¹H NMR of **1b**. ¹H NMR (400 MHz, 298 K, CDCl₃) δ 8.12 (d, 2H), 7.62 (t, 1H), 7.49 (d, 2H).

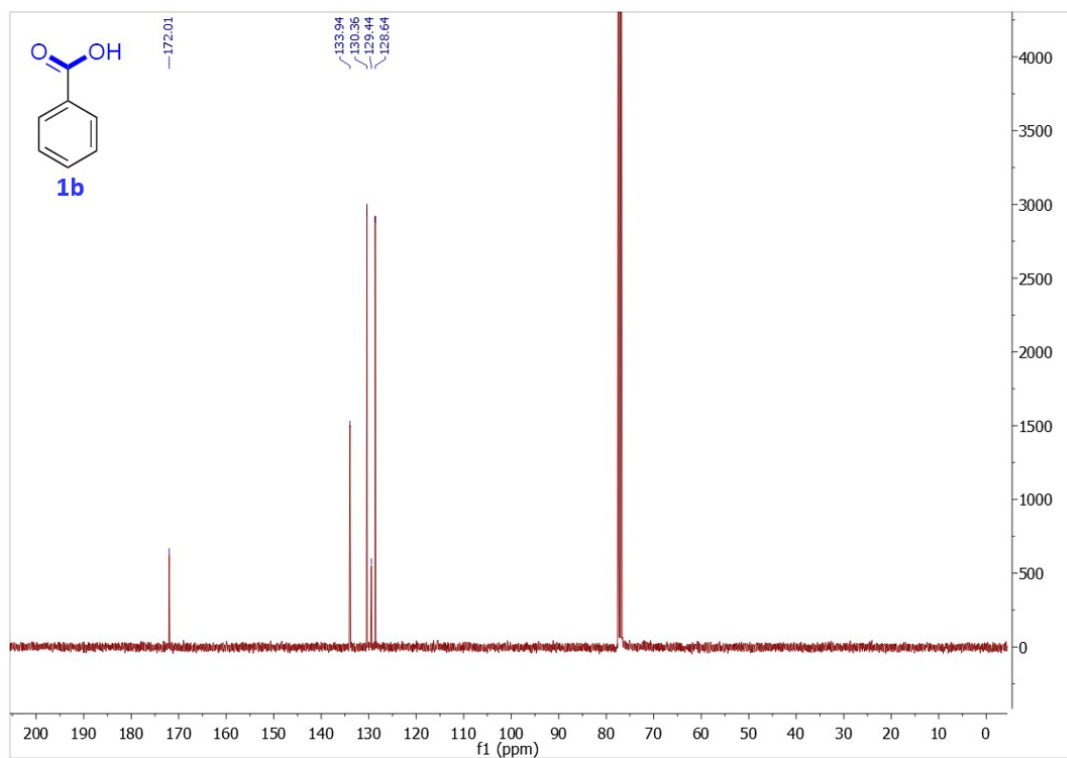


Figure S26. ¹³C NMR of **1b**. ¹³C NMR (101 MHz, 298 K, CDCl₃) δ 172.01, 133.94, 130.36, 129.44, 128.64.

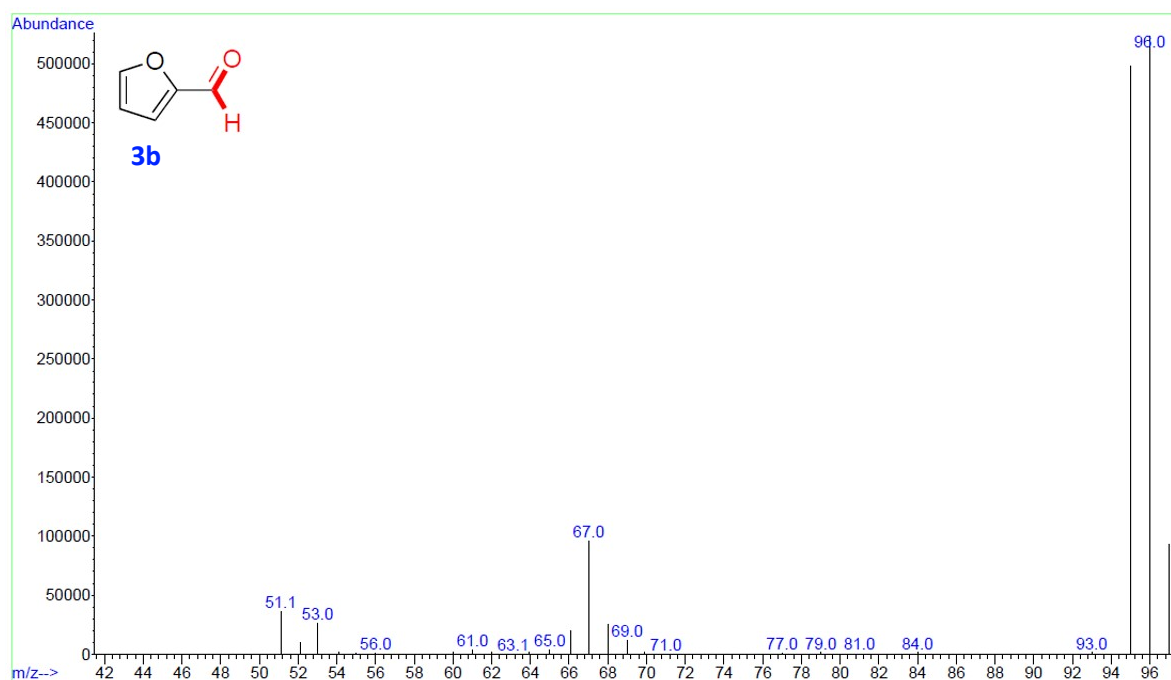


Figure S27. Mass Spectrum of **3b** (EI, 70 eV).

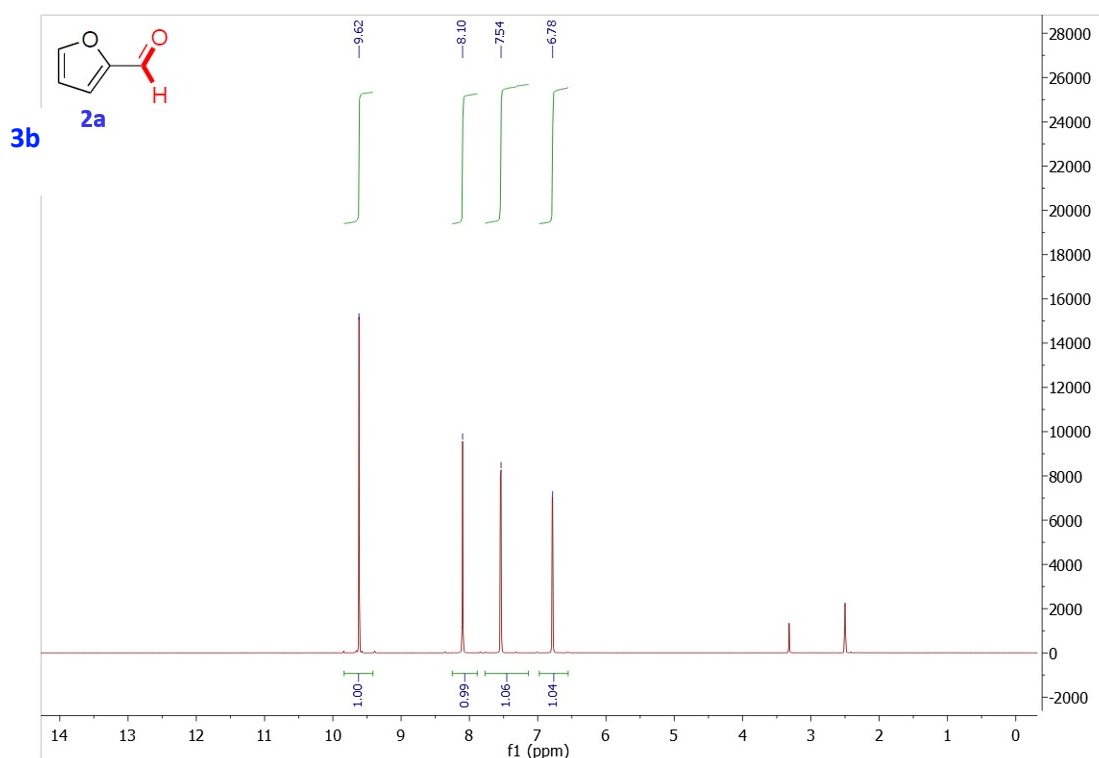


Figure S28. ^1H NMR of **3b**. ^1H NMR (400 MHz, 298 K, CDCl_3) δ 9.62 (s, 1H), 8.10 (d, 1H), 7.54 (t, 1H), 6.78 (d, 1H).

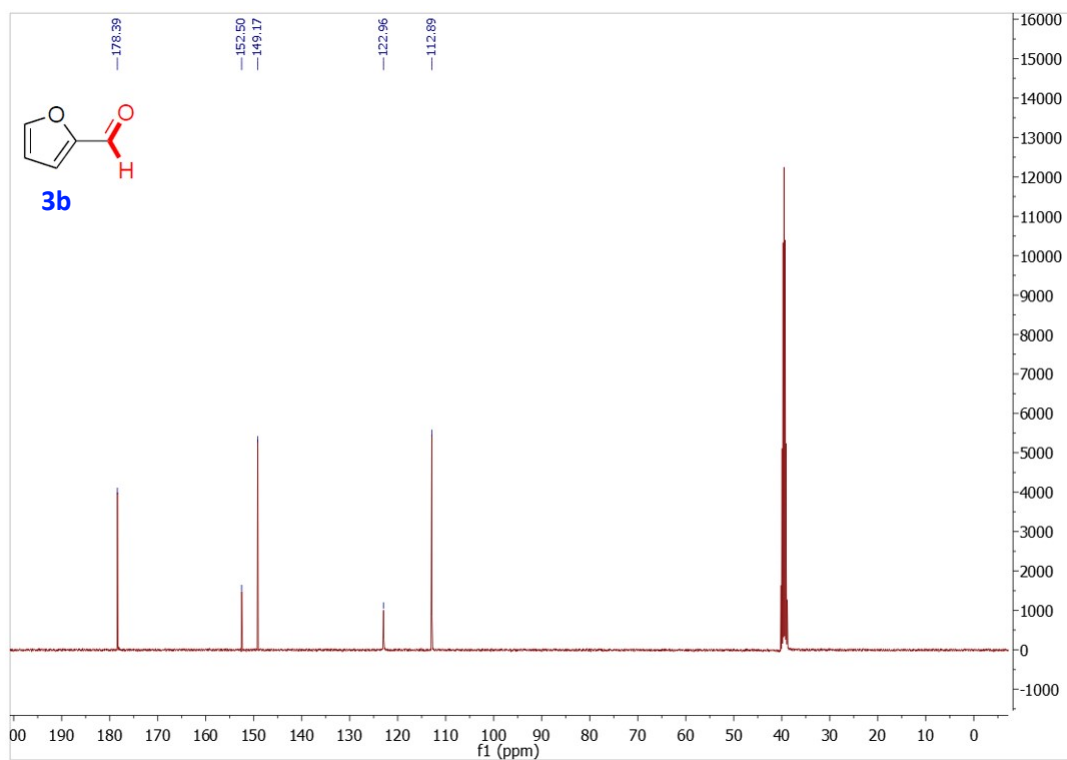


Figure S29. ^{13}C NMR of **3b**. ^{13}C NMR (101 MHz, 298 K, CDCl_3) δ 178.39, 152.50, 149.17, 122.96, 112.89.

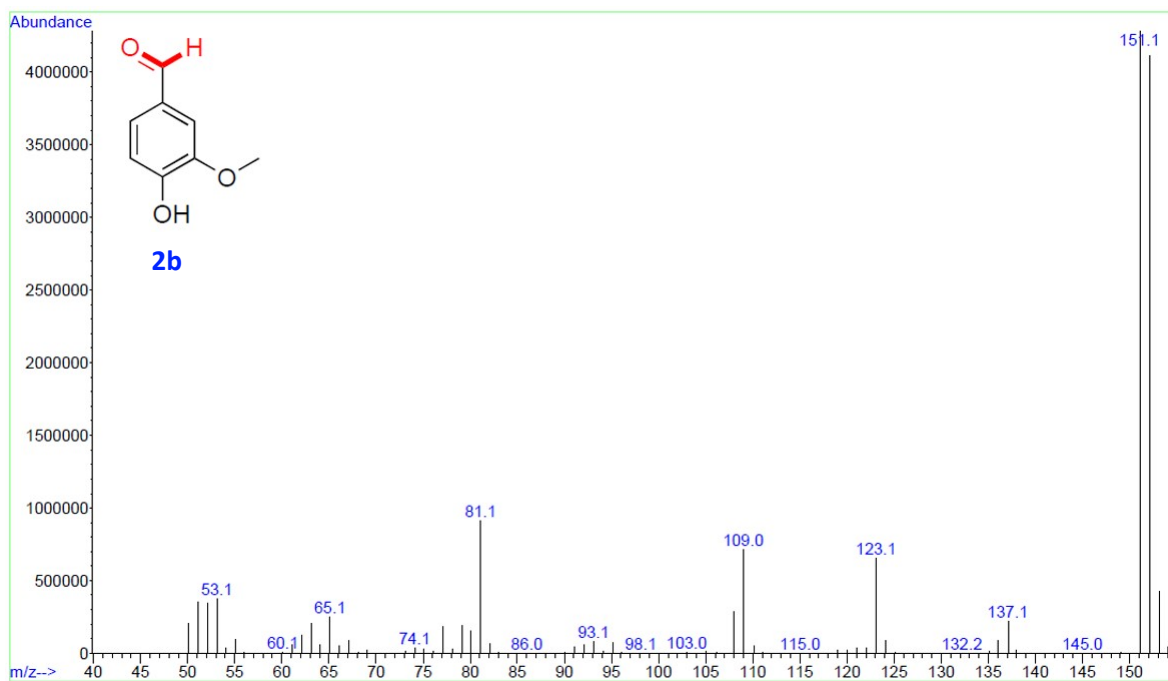


Figure S30. Mass Spectrum of **2b** (EI, 70 eV).

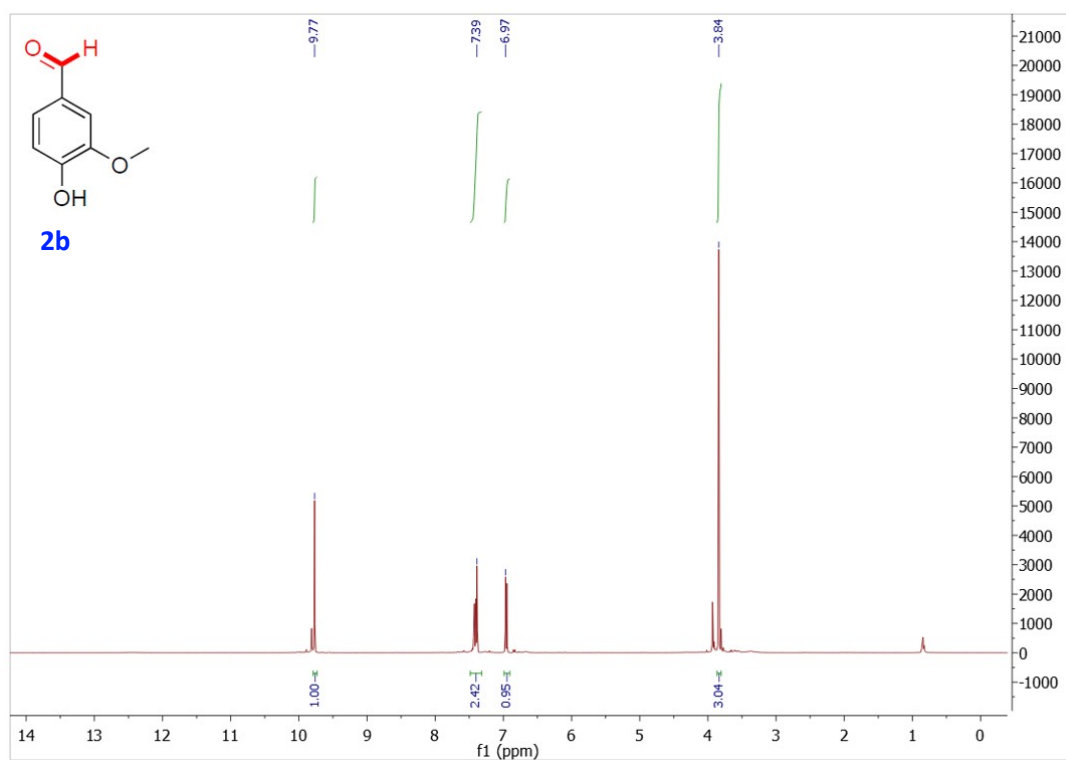


Figure S31. ^1H NMR of **2b**. ^1H NMR (400 MHz, 298 K, CDCl_3) δ 9.77 (s, 1H), 7.39 (m, 2H), 6.97 (s, 1H), 3.84 (s, 3H).

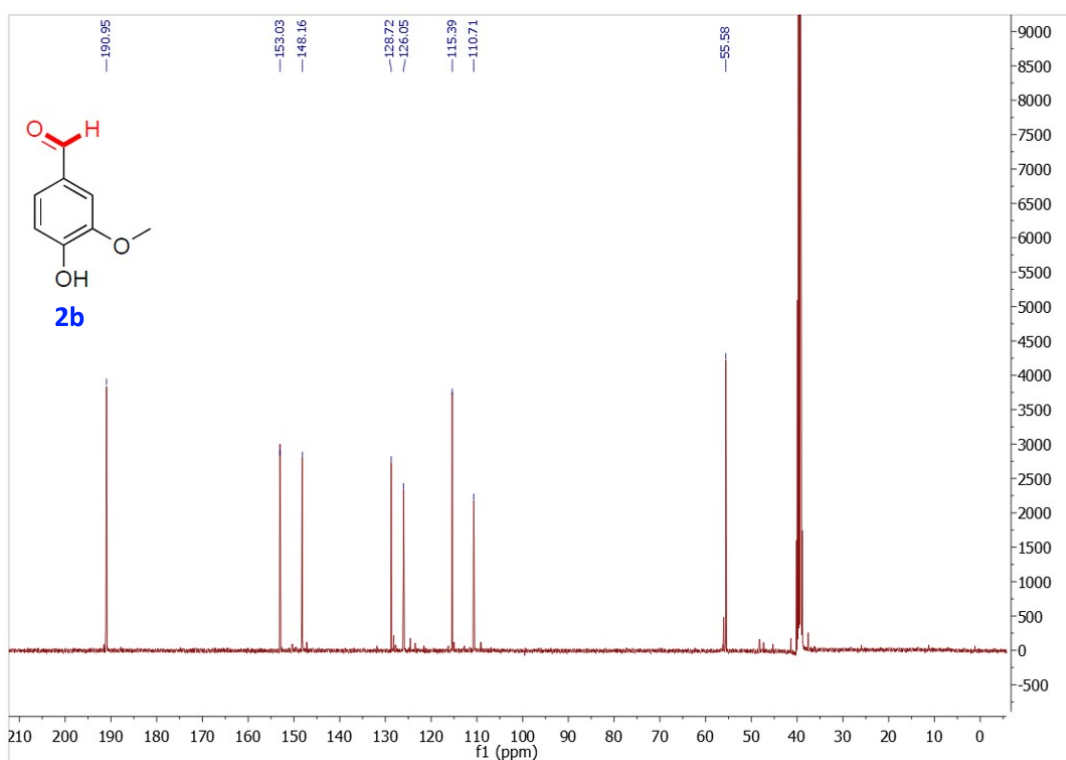


Figure S32. ^{13}C NMR of **2b**. ^{13}C NMR (101 MHz, 298 K, CDCl_3) δ 190.95, 153.03, 148.16, 128.72, 126.05, 115.39, 110.71, 55.58.

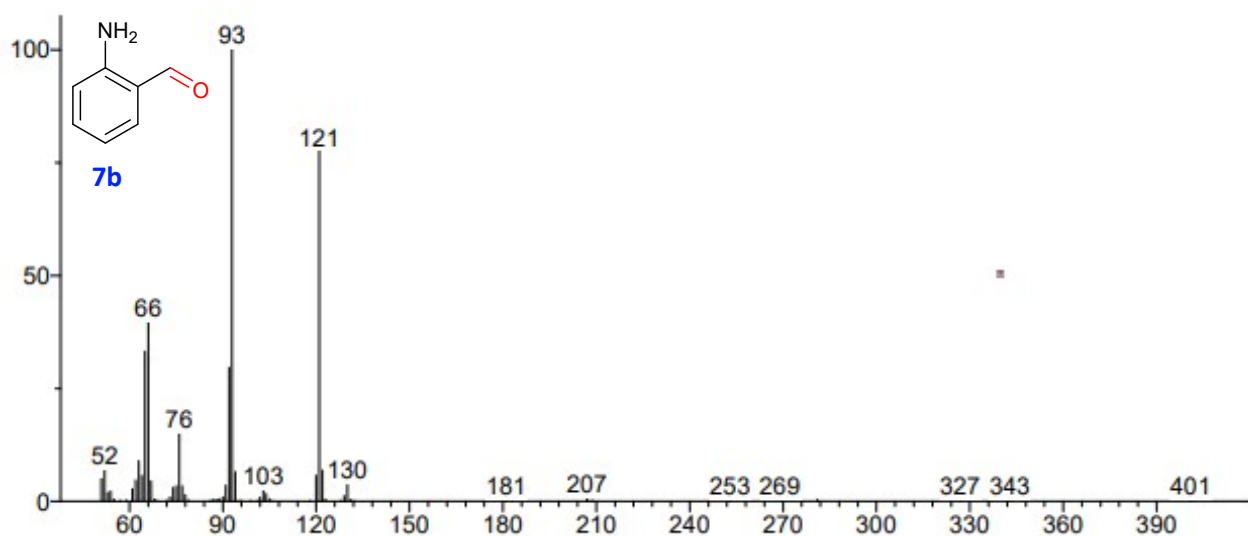


Figure S33. Mass Spectrum of **7b** (EI, 70 eV).

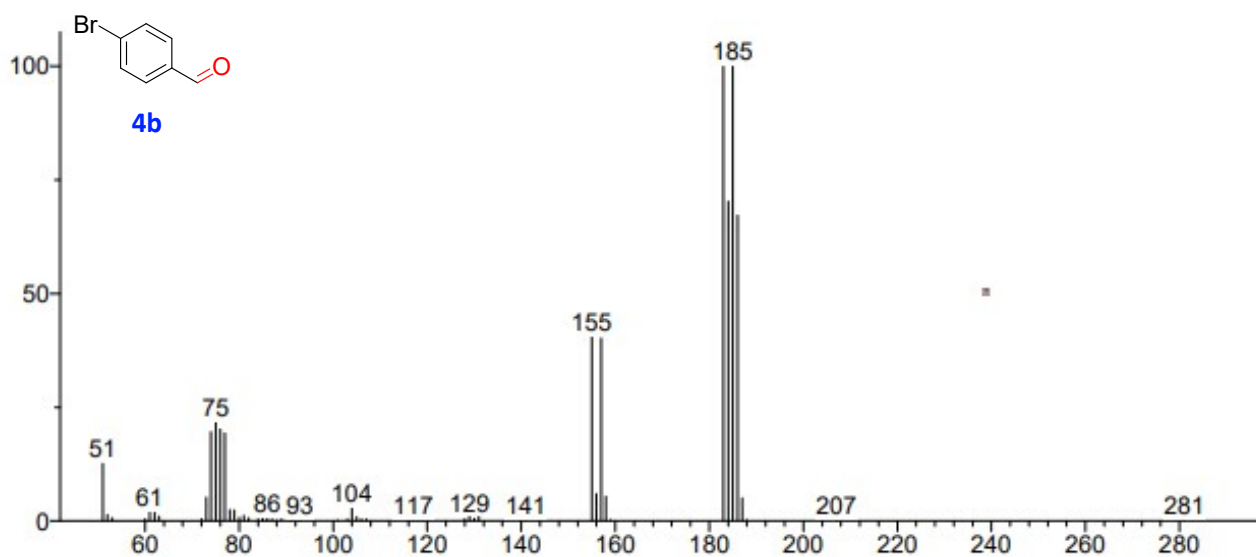


Figure S34. Mass Spectrum of **4b** (EI, 70 eV).

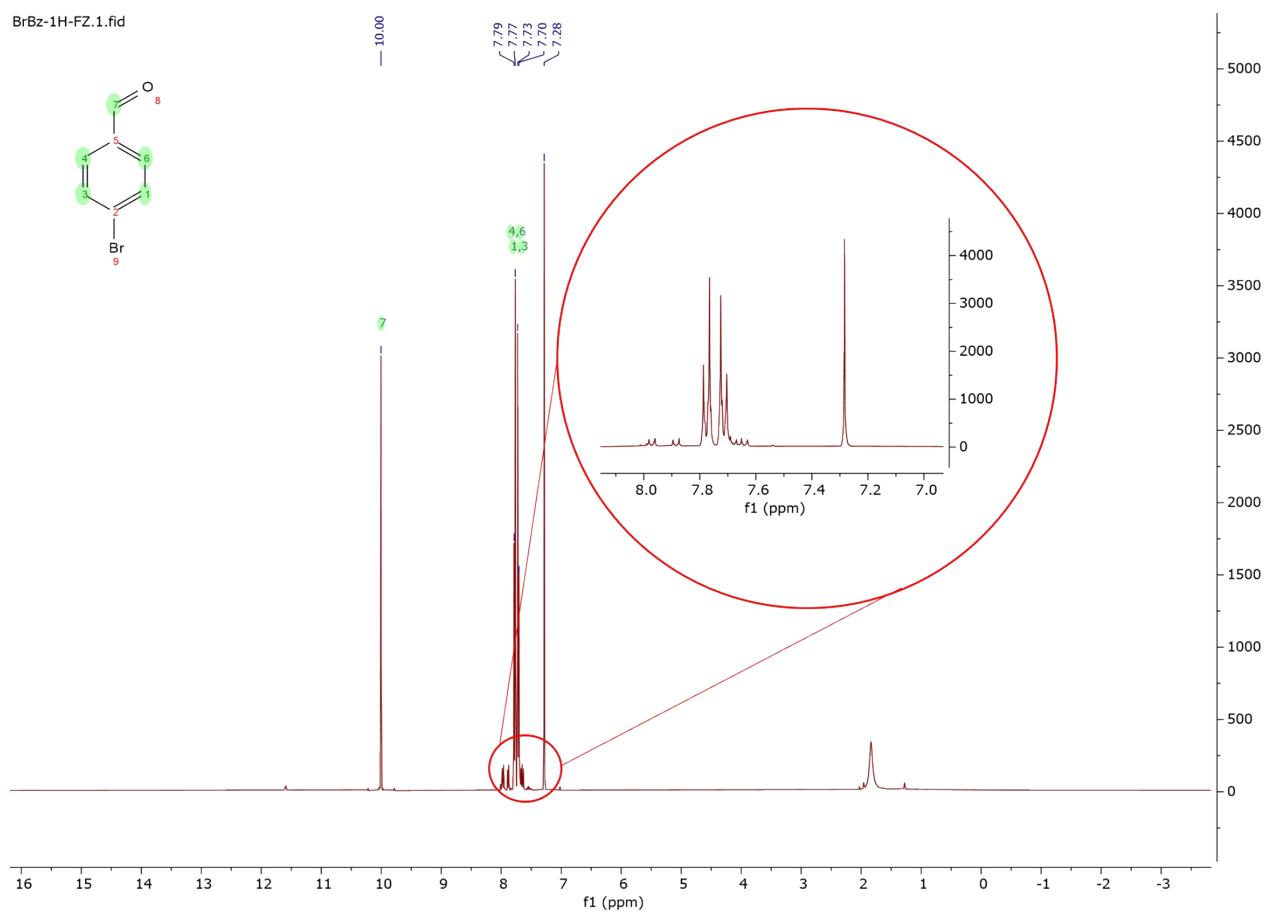


Figure S35. ^1H NMR of **4b**. ^1H NMR (400 MHz, 298 K, CDCl_3). δ 10.00, 7.77, 7.79, 7.73, 7.70.

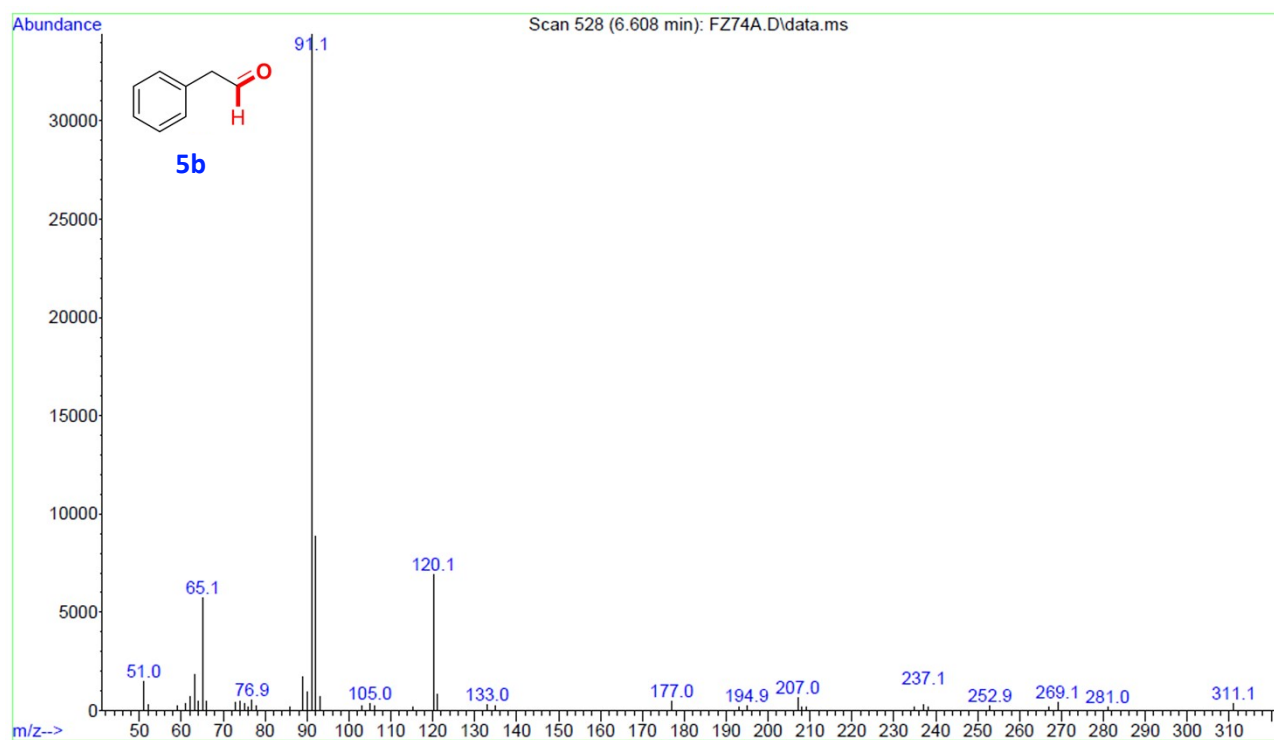


Figure S36. Mass Spectrum of **5b** (EI, 70 eV).

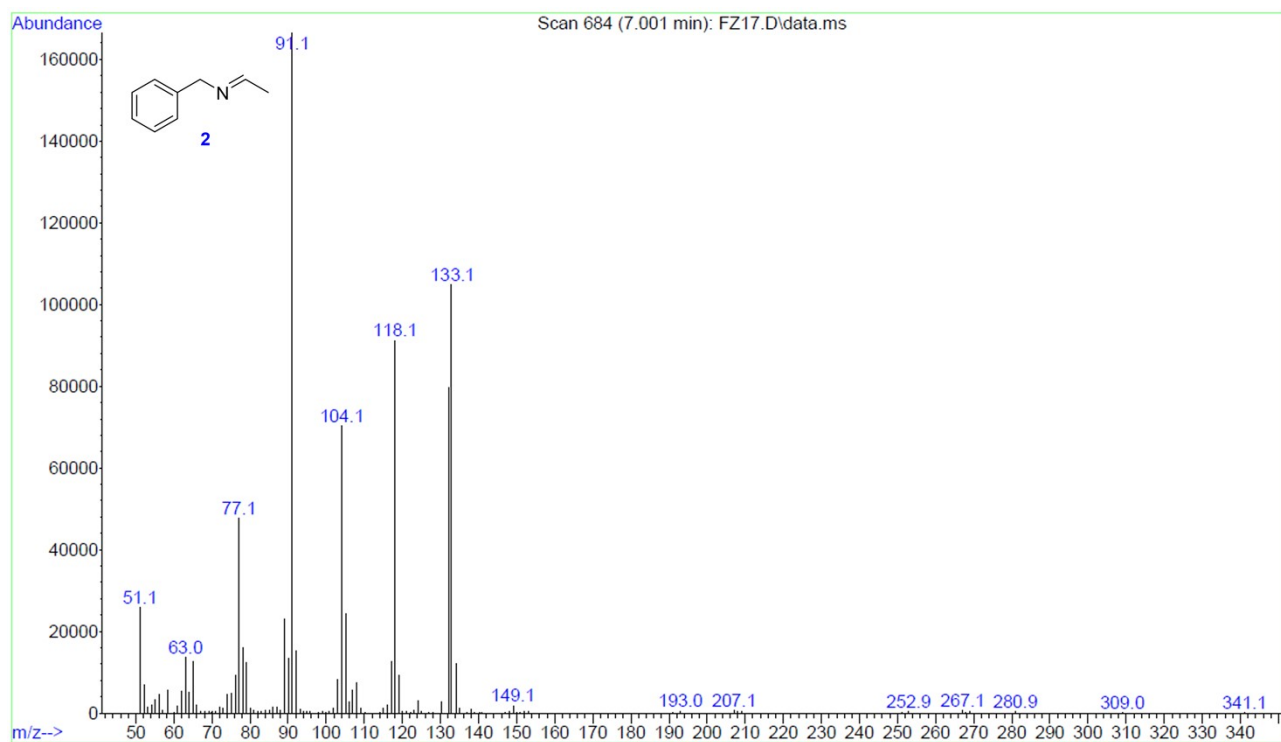


Figure S37. Mass Spectrum of **2** (EI, 70 eV).

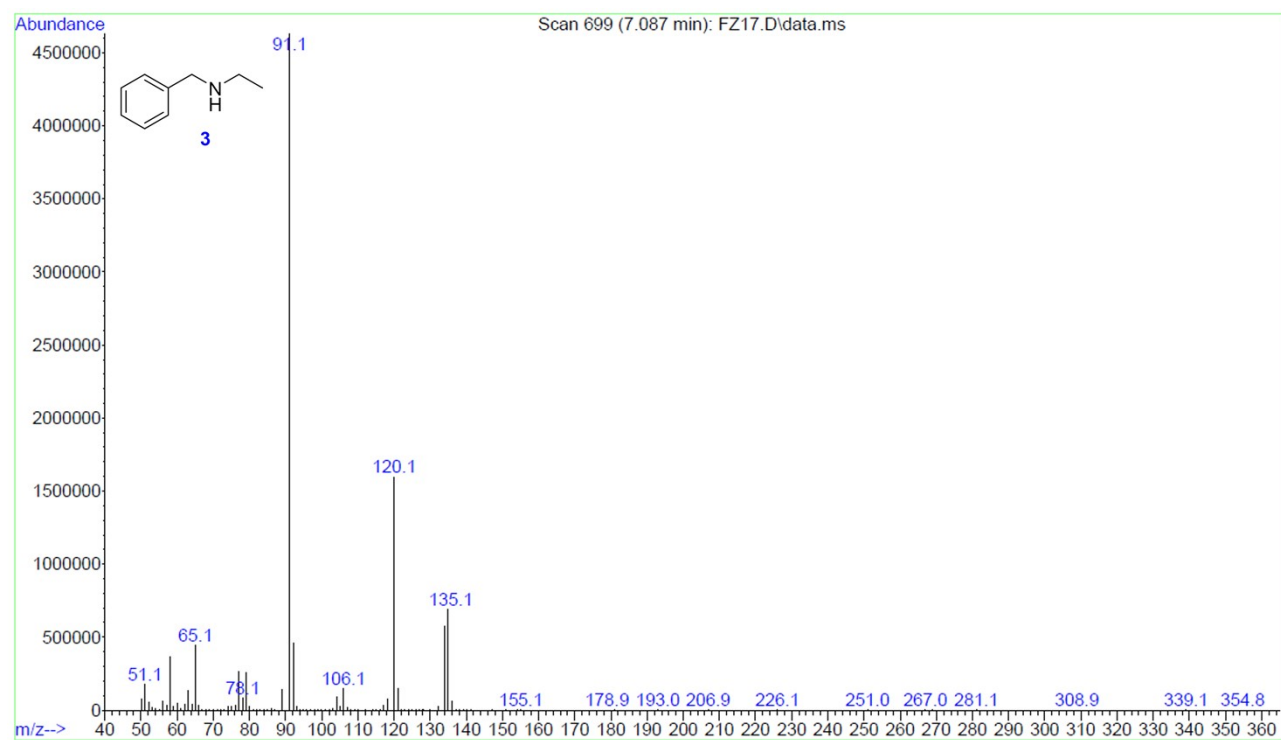


Figure S38. Mass Spectrum of **3** (EI, 70 eV).

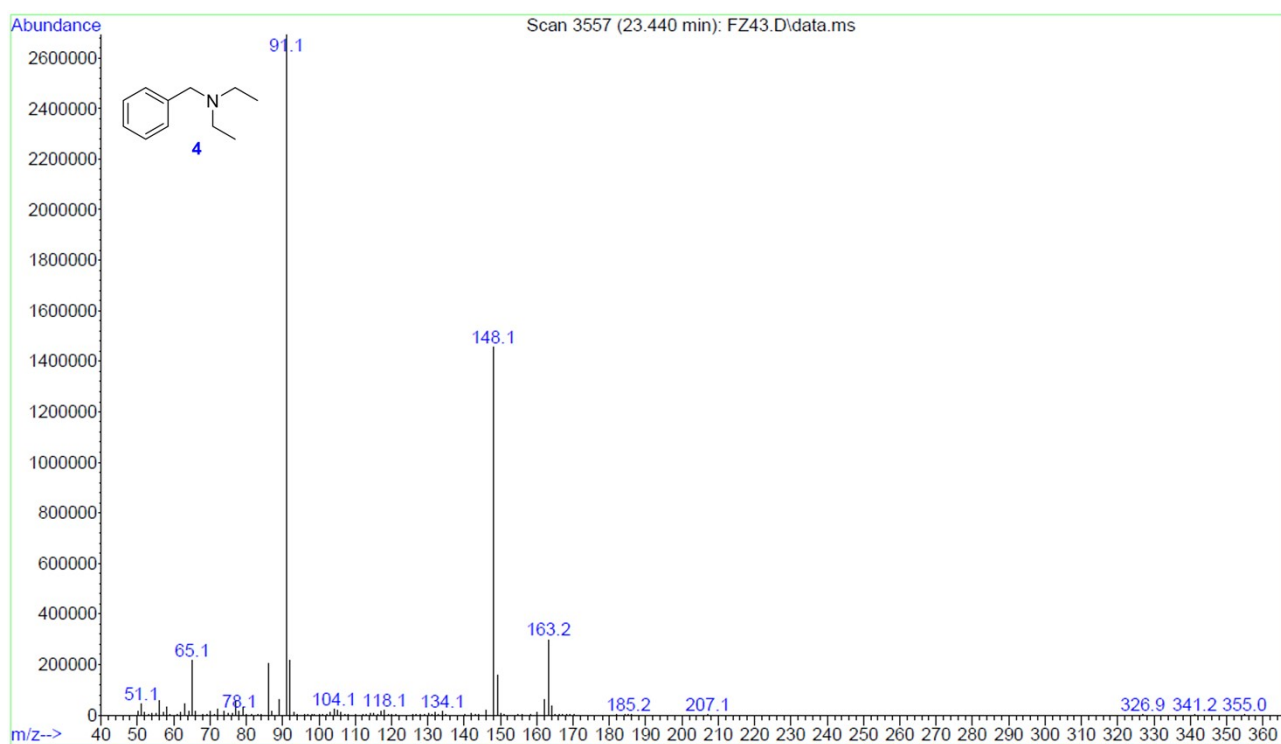


Figure S39. Mass Spectrum of **4** (EI, 70 eV).

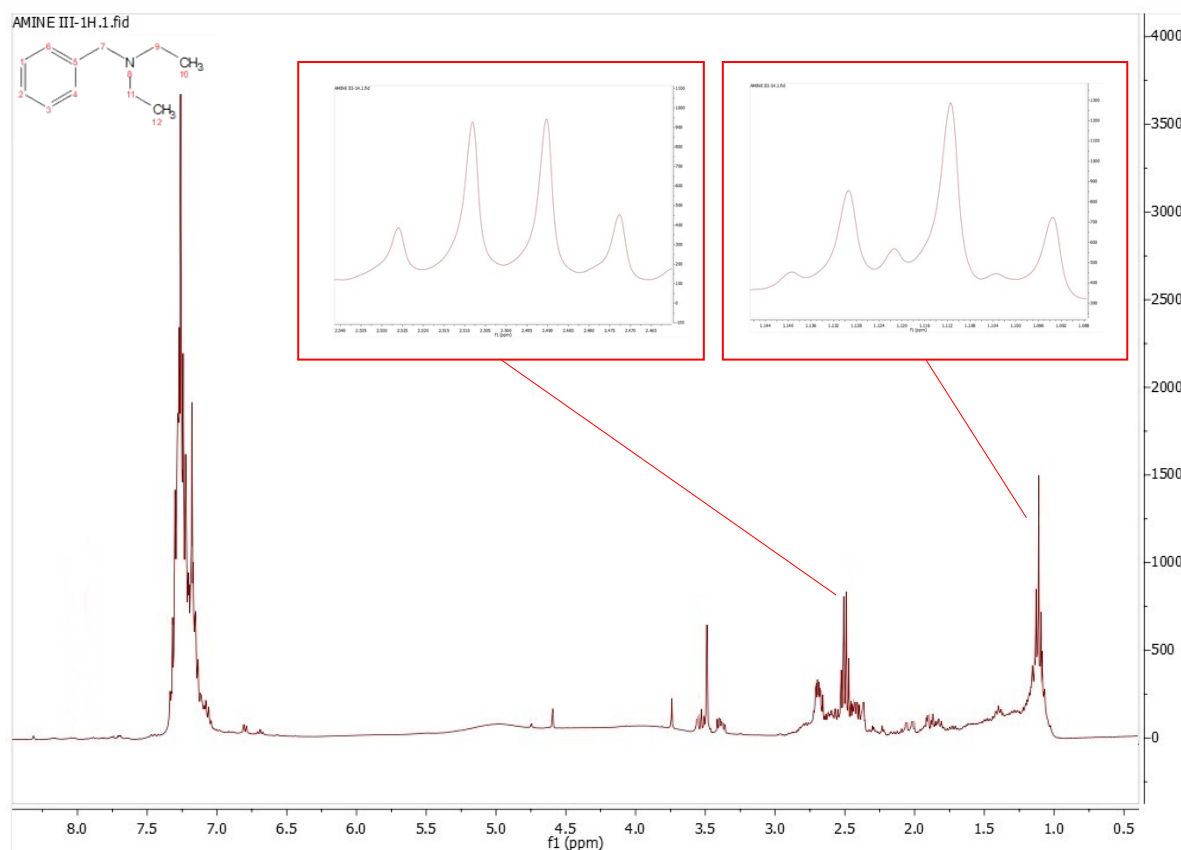


Figure S40. ^1H NMR of **4**. ^1H NMR (400 MHz, 298 K, CDCl_3)

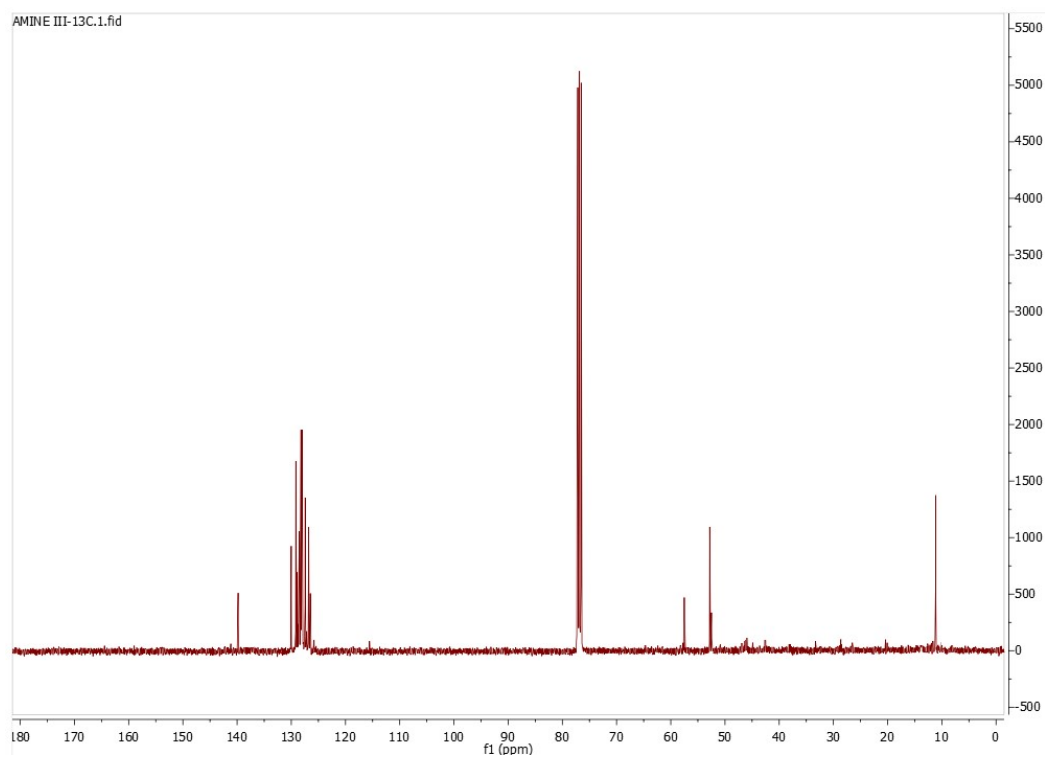


Figure S41. ^{13}C NMR of **4**. ^{13}C NMR (101 MHz, 298 K, CDCl_3)

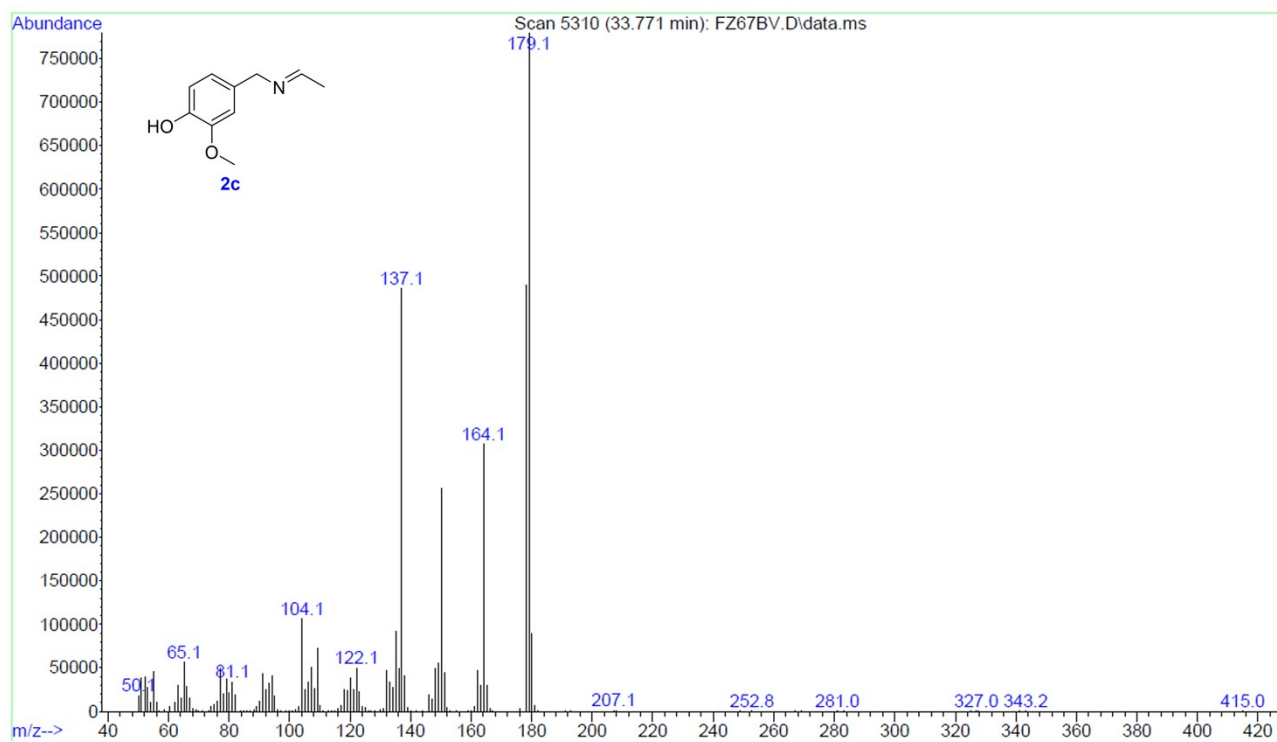


Figure S42. Mass Spectrum of **2c** (EI, 70 eV).

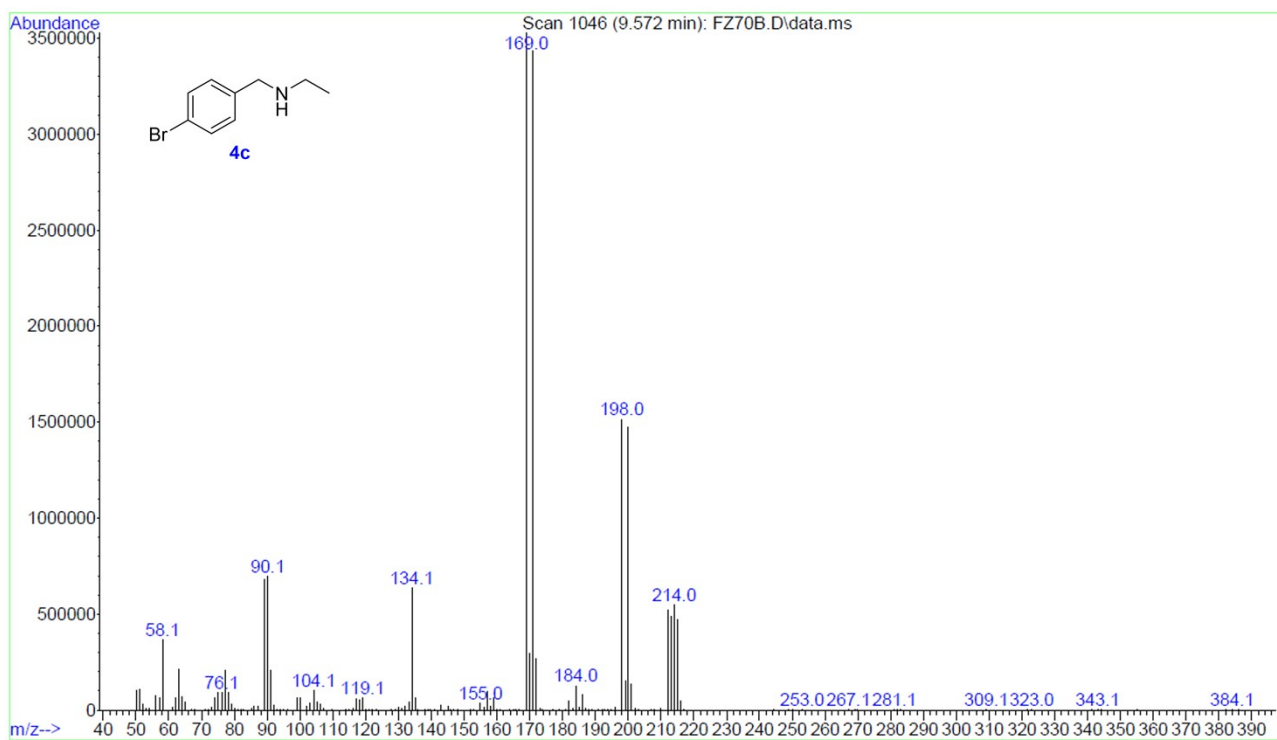


Figure S43. Mass Spectrum of **4c** (EI, 70 eV).

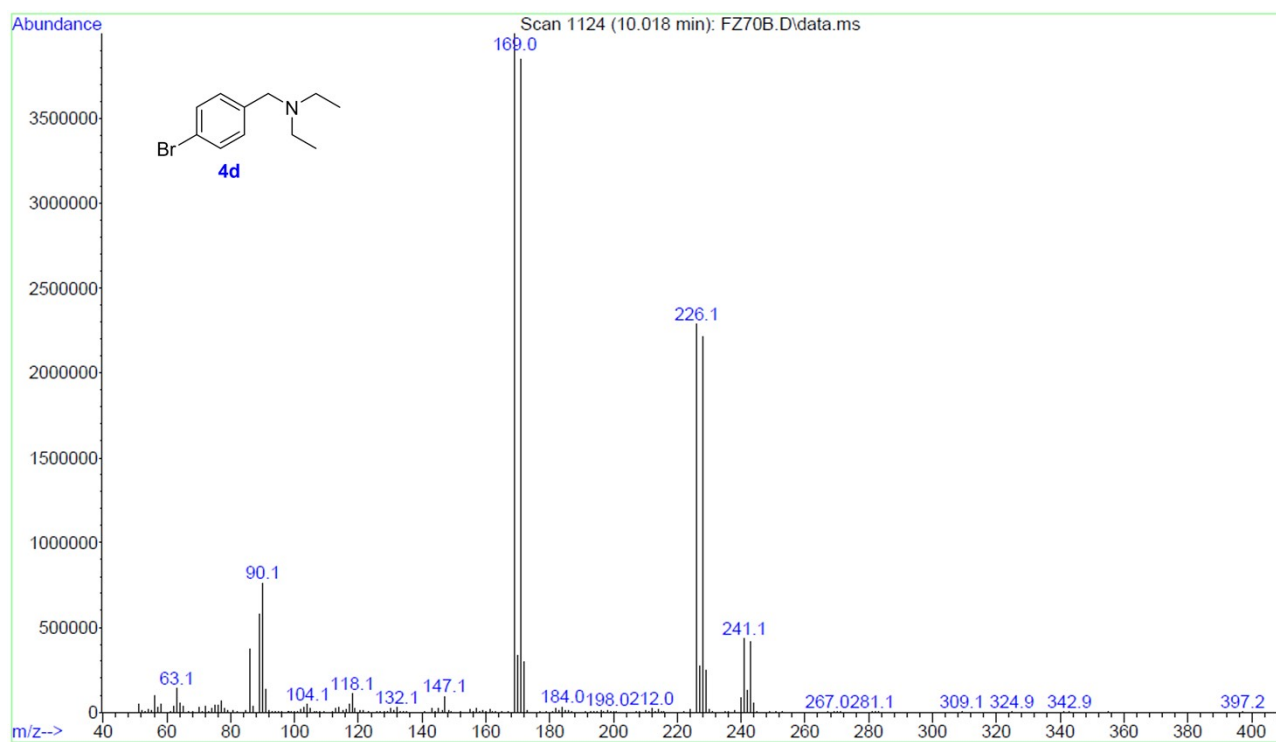


Figure S44. Mass Spectrum of **4d** (EI, 70 eV).

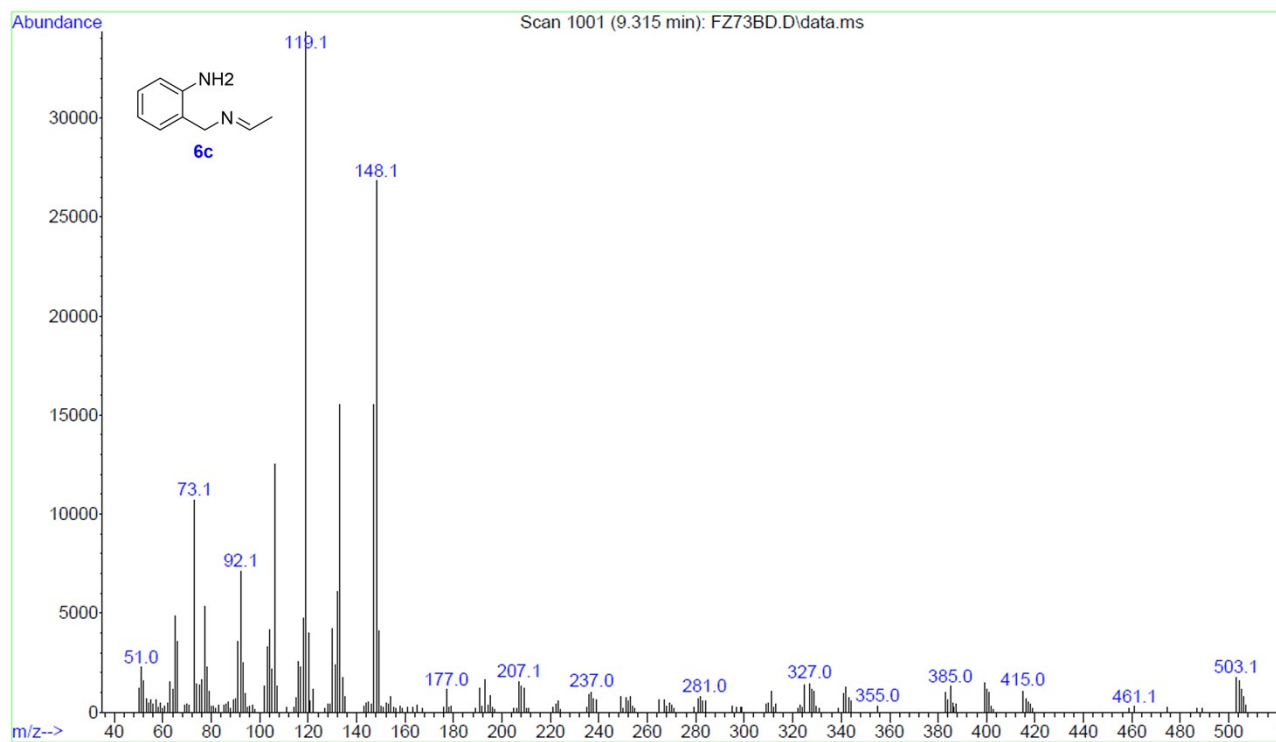


Figure S45. Mass Spectrum of **6c** (EI, 70 eV).

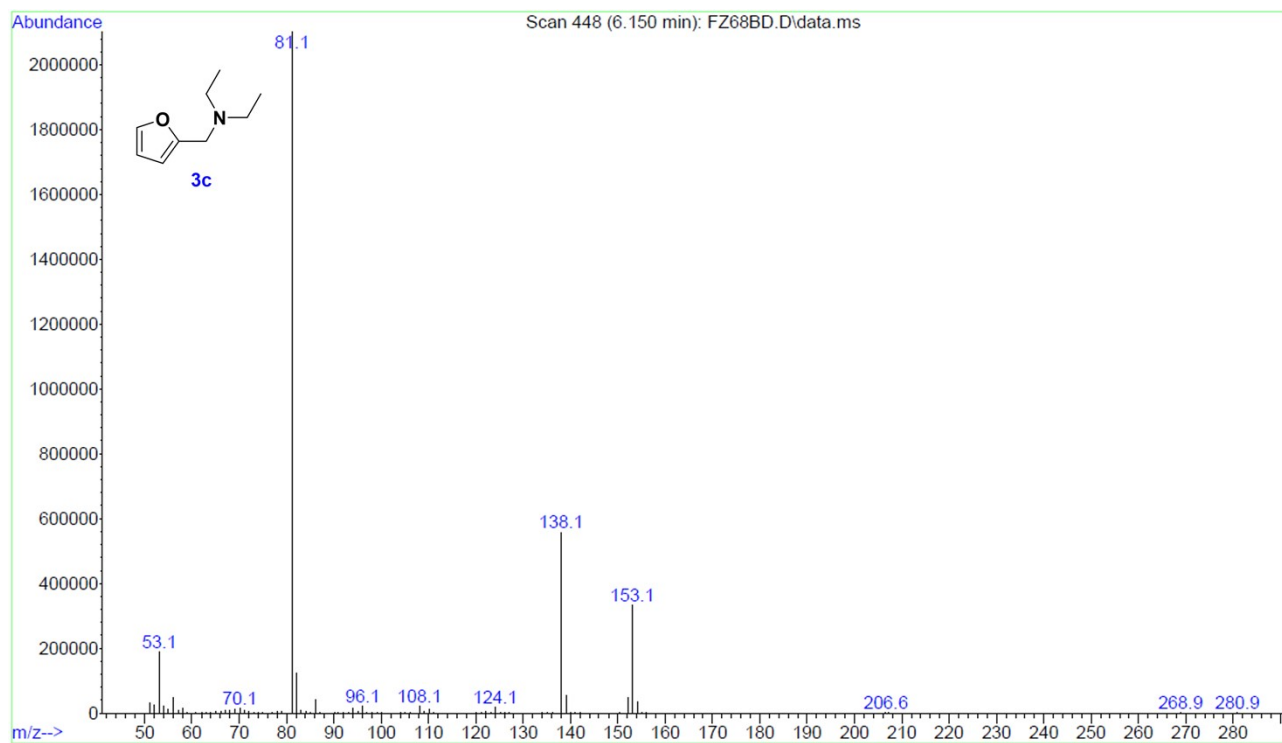


Figure S46. Mass Spectrum of **3c** (EI, 70 eV).

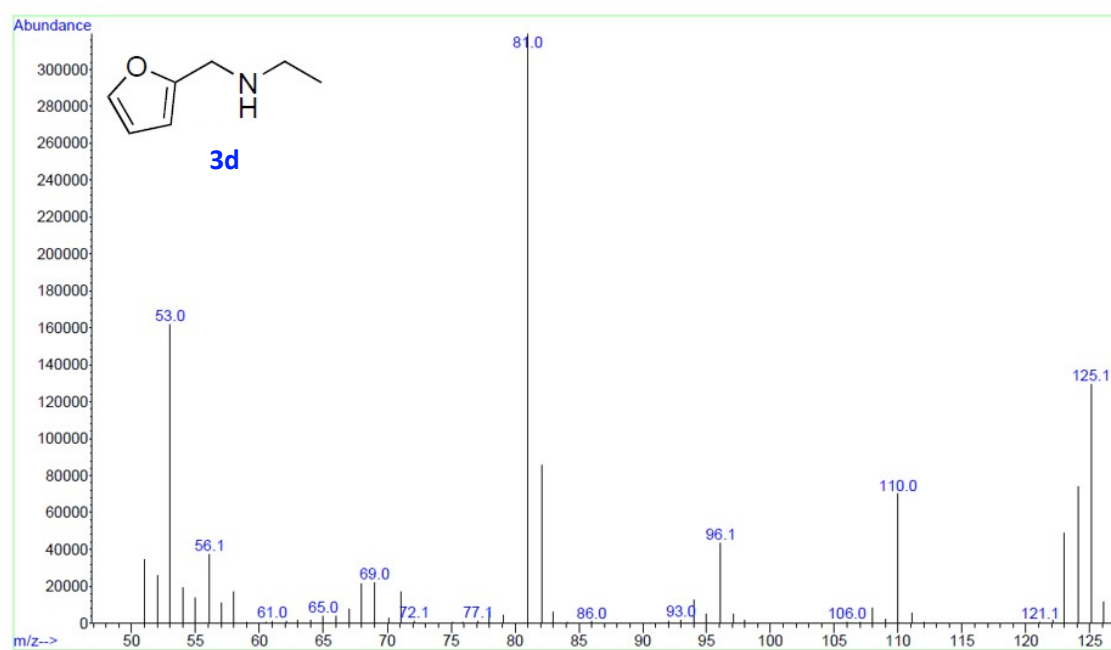


Figure S47: Mass Spectrum of **3d** (EI, 70eV).

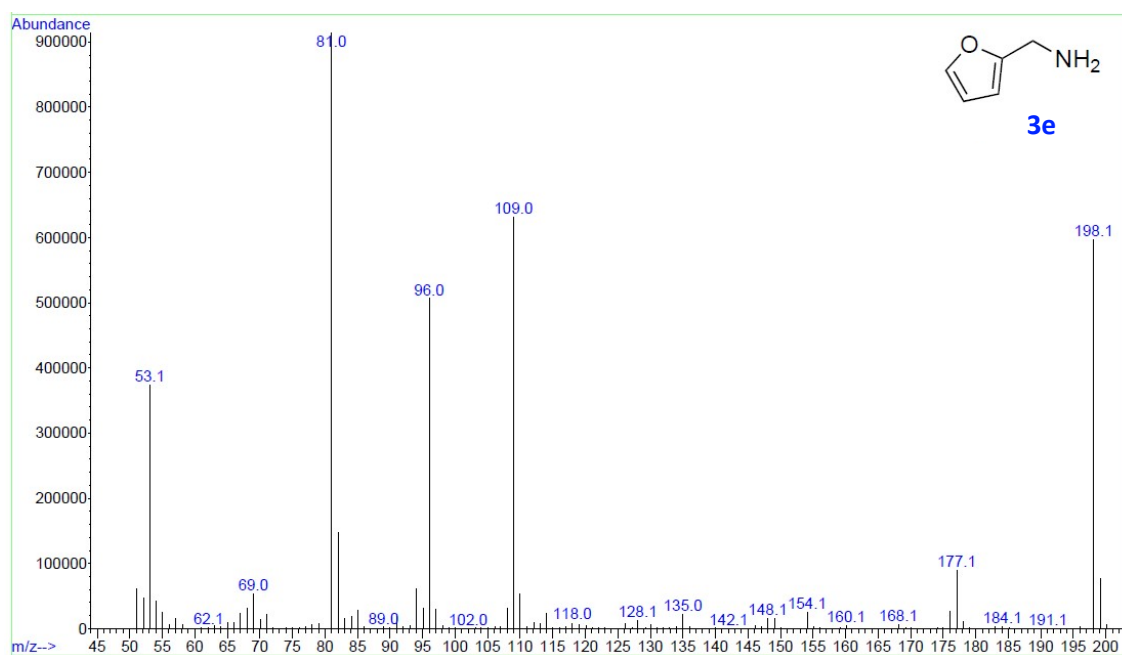


Figure S48: Mass Spectrum of **3e** (EI, 70eV).

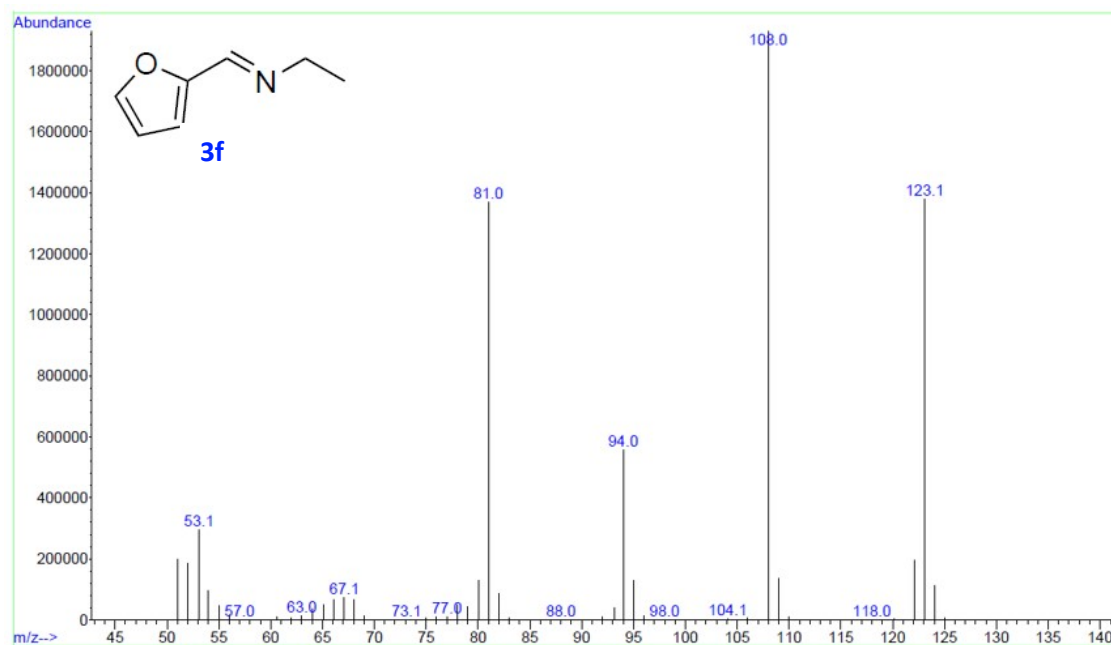


Figure S49: Mass Spectrum of **3f** (EI, 70eV).

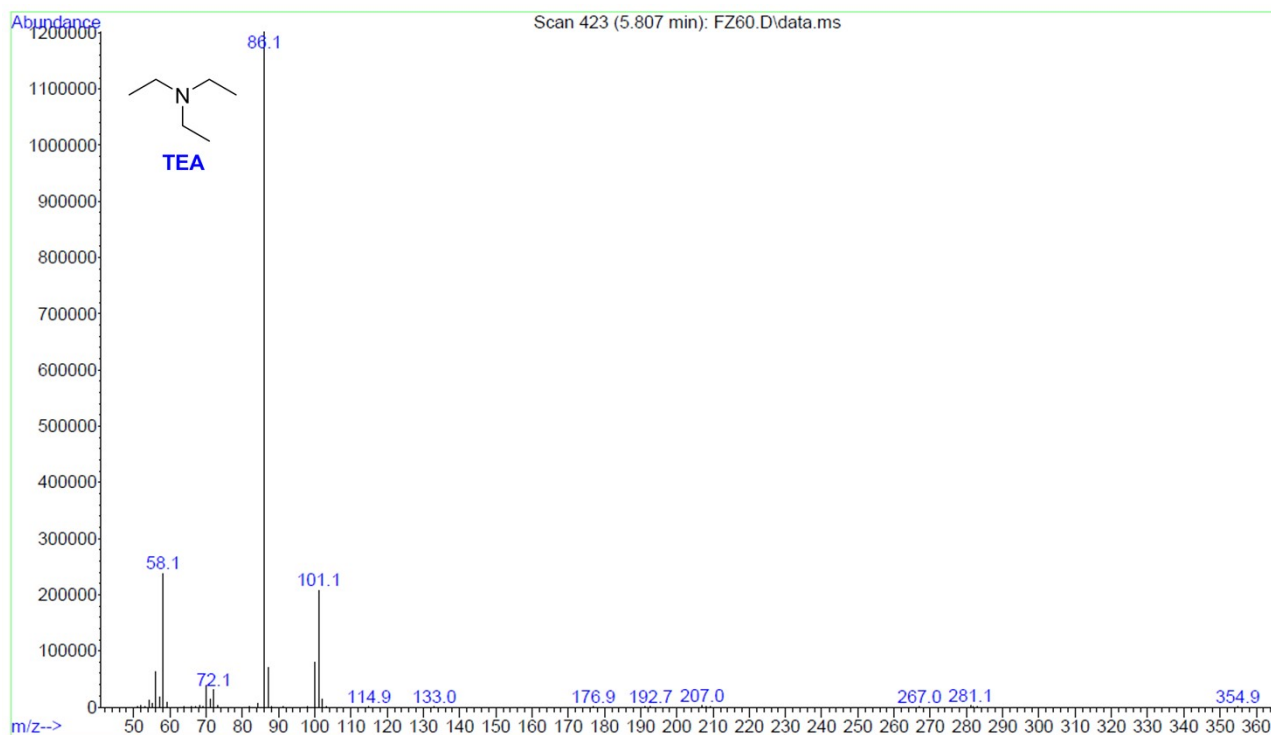


Figure S50: Mass Spectrum of *triethylamine (TEA)* (EI, 70eV).

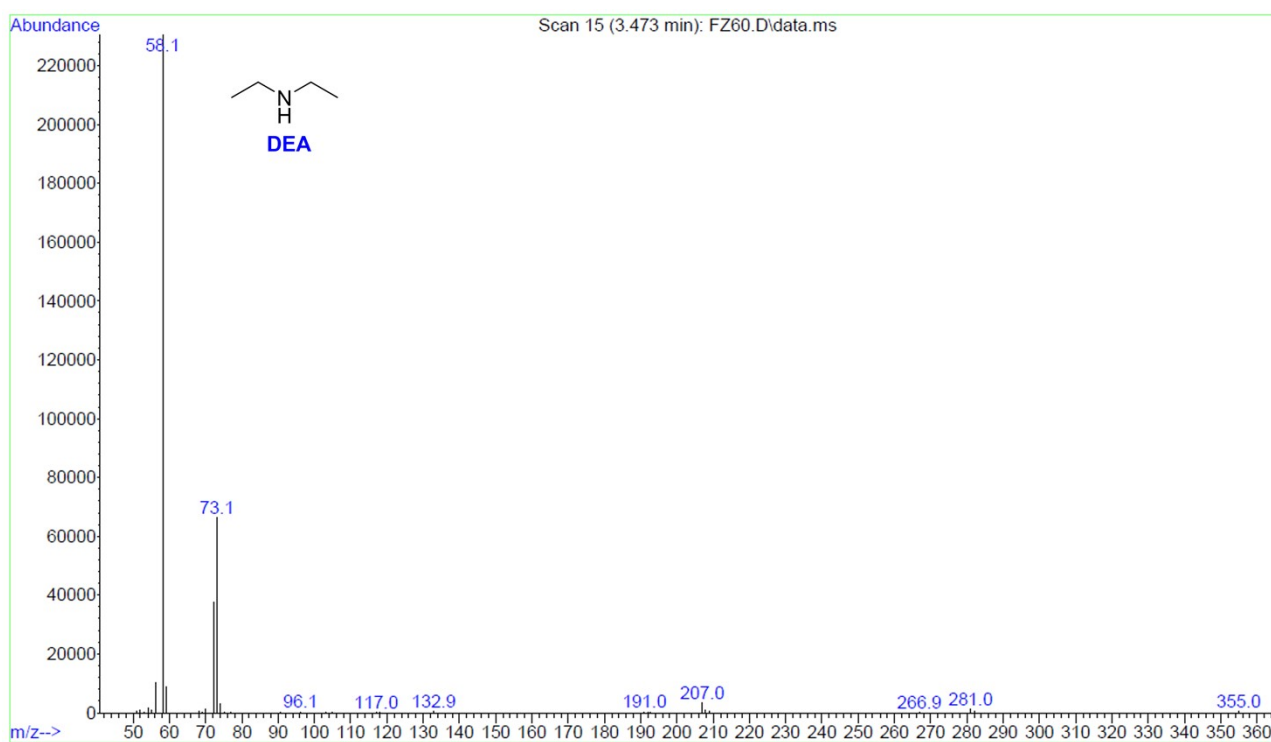


Figure S51: Mass Spectrum of *diethylamine (DEA)* (EI, 70eV).

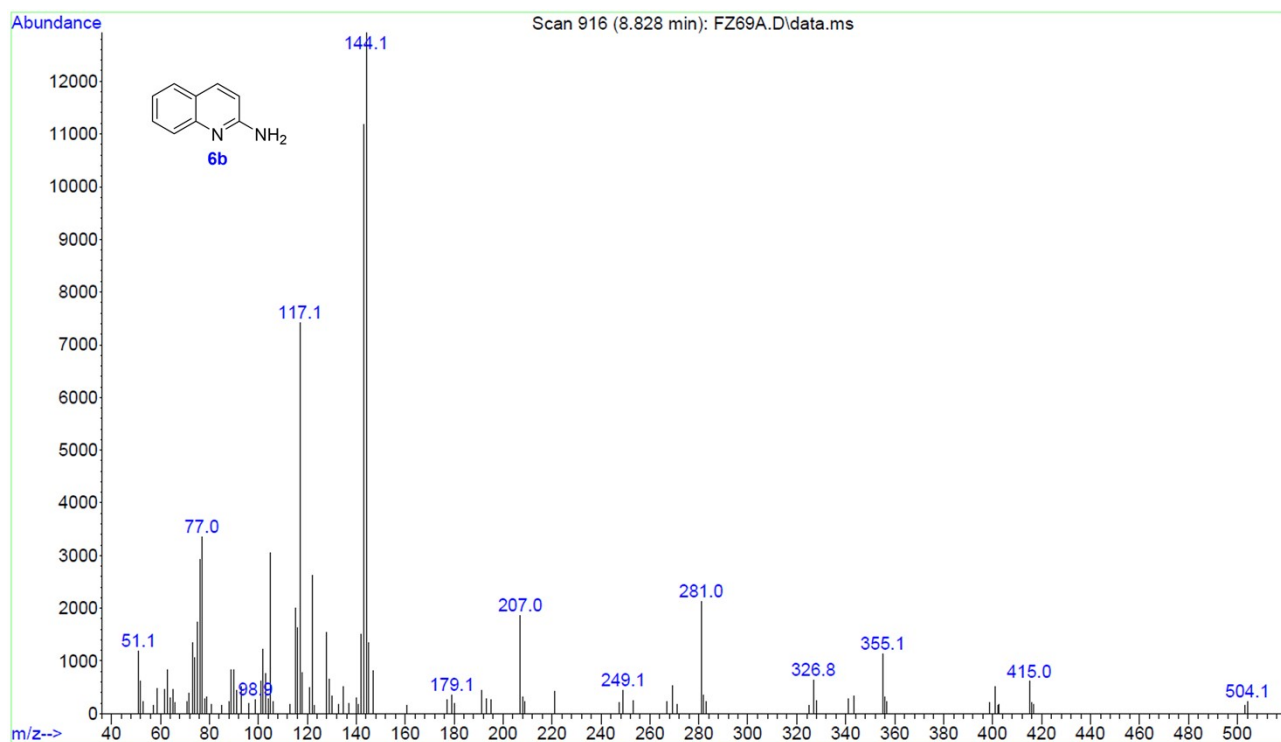


Figure S52: Mass Spectrum of **6b** (EI, 70eV).

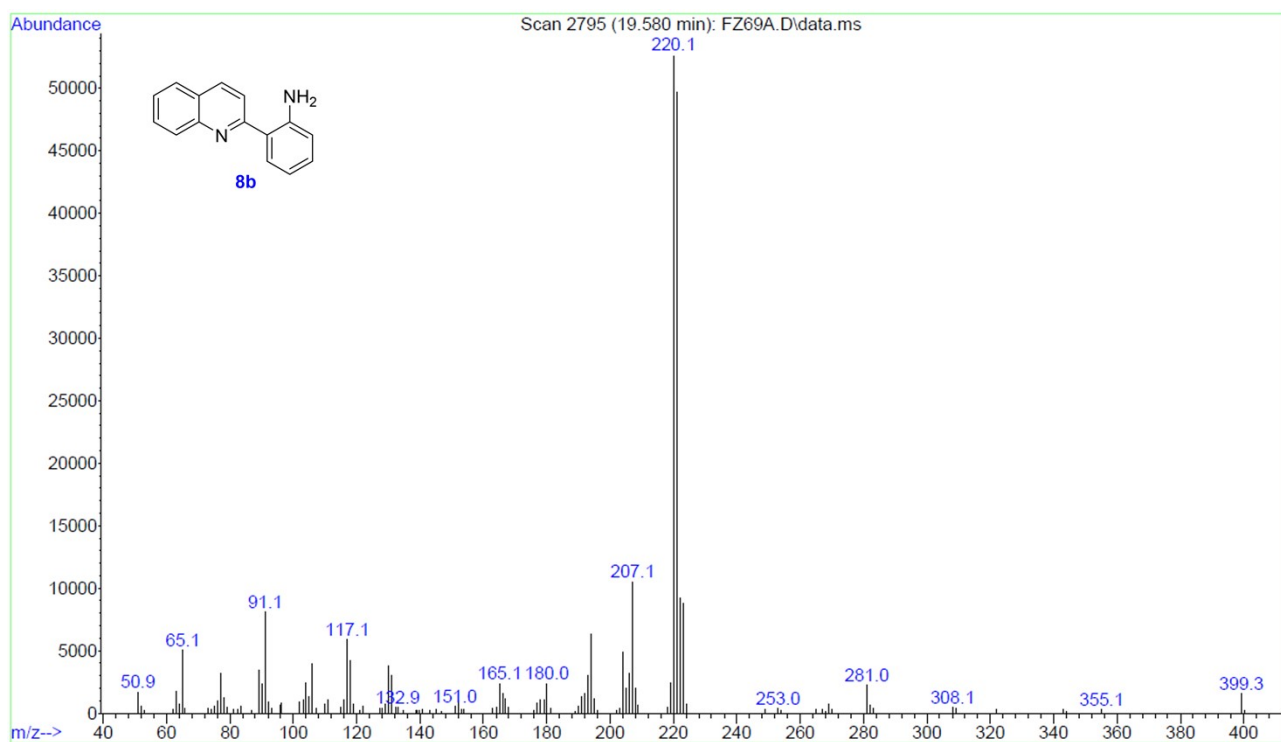
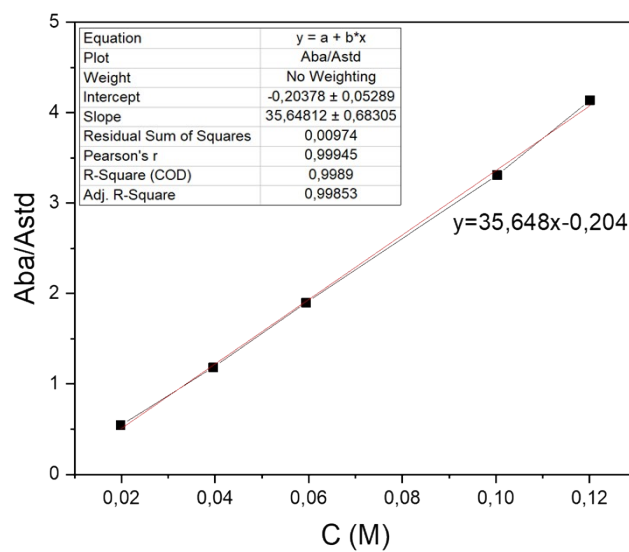


Figure S53: Mass Spectrum of **8b** (EI, 70eV).

- **Calibration curve**



• **Figure S54:** calibration curve made with GC-FID analyses (standard used: Benzaldehyde).